

1 Responses of estuarine circulation to the morphological evolution in a
2 convergent, microtidal estuary

3 Rui Zhang^a, Bo Hong^b, Lei Zhu^{a,c,d}, Wenping Gong^{a,c*}, Heng Zhang^{a,c,d}

4 a- School of Marine Sciences, SunYat-sen University, Guangzhou, China, 510275

5 b- School of Civil Engineering and Transportation-~~Engineering~~, South China University
6 of Technology, Wushan RD., Tianhe District, Guangzhou 510641, China

7 c- Southern Marine Science and Engineering Guangdong Laboratory (Zhuhai), Zhuhai
8 519000, China

9 d- Pearl River Estuary Marine Ecosystem Research Station, Ministry of Education,
10 Zhuhai, 519082, China

11
12 **Abstract:**

13 The Huangmaohai Estuary (HE) is a funnel-shaped microtidal estuary in the west
14 of the Pearl River Delta (PRD) in southern China. Since China's reform and opening up
15 in 1978, extensive human activities have occurred and greatly changed the estuary's
16 topography, and modified its hydrodynamics. In this study, we examined the
17 morphological evolution by analyzing remote sensing data with ArcGIS tools and
18 studied the responses of hydrodynamics to the changes in topography from 1977 to
19 2010 by using the Delft3d model. We took the changes in estuarine circulation during
20 neap tides in dry seasons as an example. The results show that human reclamation
21 caused a narrowing of the estuary, and channel dredging deepened the estuary. These
22 human activities changed both the longitudinal and lateral estuarine circulations. The
23 longitudinal circulation was observed to increase with the deepening and narrowing of
24 the estuary. The lateral circulation experienced changes in both the magnitude and
25 pattern. The momentum balance analysis shows that when the depth and width changed
26 simultaneously, the longitudinal estuarine circulation was modulated by both the

* Supported by the National Natural Science Foundation of China under contract Nos 51761135021,
41506102 and 41890851.

** Corresponding author, E-mail: gongwp@mail.sysu.edu.cn

27 channel deepening and width reduction, in which the friction, pressure gradient force,
28 and advection terms were altered. The analysis of the longitudinal vortex dynamics
29 indicates that the changes in the vertical shear of the longitudinal flow, lateral salinity
30 gradient, and vertical mixing were responsible for the change in the lateral circulation.
31 The changes in water depth are the dominant factor affecting lateral circulation intensity.
32 This study has implications for sediment transport and morphological evolution in
33 estuaries heavily impacted by human interventions.

34

35 **Keywords:** Estuarine circulation, Morphological evolution, Huangmaohai Estuary

36

37 **1. Introduction**

38

39 Estuarine circulation, the tidally averaged flow in estuaries including both the
40 longitudinal and lateral circulations, is the main driving force for the transport of
41 sediment, pollutants, and other materials, and also one of the primary factors affecting
42 the ecological environment of estuaries (Kjerfve et al., 1981). Estuarine circulation is
43 influenced by many factors (Geyer and Maccready, 2014), such as sea-level
44 fluctuations (Wilson and Filadelfo, 1986), river discharge, tides (Pritchard, 1952), and
45 winds (Scully et al., 2005; Waterhouse et al., 2013; Geyer and Maccready, 2014; Salles
46 et al., 2015; Chen et al., 2020a). Topography in an estuary has a significant effect on
47 the pattern and intensity of the estuarine circulation (Fischer, 1976; Dyer, 1977).
48 Human activities may change the estuarine topography, leading to changes in the
49 estuarine circulation and associated material transport. Therefore, a study of the
50 estuarine circulation and its response to human activities is essential for integrated
51 management of the development of estuarine resources, and the maintenance of the
52 estuary's ecological health.

53 Channel deepening by dredging and sand mining is a common practice in the
54 development and maintenance of navigable channels in estuaries. Generally speaking,
55 channel deepening can increase the longitudinal estuarine circulation by decreasing the

56 bottom friction and increasing the baroclinic forcing which is proportional to the water
57 depth (Amin, 1983; Chernetsky et al., 2010; Winterwerp, 2011). On the other hand, the
58 increase in water depth can also increase the salt intrusion and decrease the along-
59 channelhorizontal-density gradient, thus reducing the baroclinic forcinge. Channel
60 deepening also affects the estuarine circulation in other ways, such as increasing the
61 Stokes transport and the associated compensating return flow (Amin, 1983), altering
62 the nonlinear tidal rectification (Li and O'Donnell, 1997), and tidal asymmetry in
63 mixing between flood and ebb tides (tidal straining) (Simpson, 1990). Therefore, the
64 effect of channel deepening is an intricate balance between these reinforcing and/or
65 competing effects. Chant et al. (2018) demonstrated that a relatively small (15%)
66 increase in water depth can result in a double exchange flow. They attributed this
67 increase to the increase in along-channelhorizontal salinity gradient and/or a reduction
68 in vertical mixing, but they did not give a clear distinction about how these two effects
69 work together and which is dominant.

70 Change in estuary width is another aspect of topographic change in estuaries and
71 is mainly caused by reclamation and utilization of salt marshes, construction of coastal
72 protection structures along the estuarine banks. Change in estuary width generates a
73 change in the estuarine convergence, and therefore a change in the estuarine circulation.
74 Burchard et al. (2014) concluded that an increase in the estuarine convergence results
75 in an enhancement or reduction of the longitudinal estuarine circulation as increased
76 estuarine convergence can reduce or even reverse the straining-induced circulation,
77 though the advection-induced circulation is increased. Changes in estuarine width can
78 also modify the lateral circulation and feedback to the generation of the longitudinal
79 estuarine circulation through the change in lateral advection (Lacy et al., 2003; Lerczak
80 and Rockwell Geyer, 2004; Scully et al., 2009; Burchard et al., 2010; Burchard et al.,
81 2014). Lerczak and Rockwell Geyer (2004) suggested that lateral effects on the
82 longitudinal estuarine circulation would be stronger in narrower estuaries given a
83 constant lateral salinity gradient. Schulz et al. (2015) investigated the impact of the
84 depth-to-width ratio of the estuarine cross-section on the longitudinal estuarine

85 circulation and found that the longitudinal estuarine circulation exhibits a distinct
86 maximum in medium-wide channels. They diagnosed the mechanisms for such a
87 phenomenon and attributed it to the sensitivities of the straining- and advection-induced
88 circulations on the changes in depth-to-width ratio.

89 As revealed by Lerczak and Geyer (2004) and other researchers (Chen et al.,
90 2020b), lateral processes play important roles in the generation of the longitudinal
91 estuarine circulation. In estuaries, the pattern and intensity of lateral circulation are
92 controlled by three processes (Li et al., 2014): vertical shear of the longitudinal current
93 affecting the tilting of planetary vorticity, lateral salinity gradient (baroclinicity), and
94 diffusion. The longitudinal estuarine circulation can affect the lateral circulation
95 through all the mentioned three factors. Therefore, the interaction between the
96 longitudinal and lateral processes is fully nonlinear and quite complex. Though these
97 interactions have been discussed in detail (Scully et al., 2009; Li et al., 2017), several
98 questions remain open: How does the longitudinal estuarine circulation affect the
99 intensity and vortex structure of the lateral circulation? Does a decreased/increased
100 lateral circulation necessarily lead to a weakened/strengthened longitudinal circulation?
101 These questions become complicated in an estuary where both width and depth vary.
102 Previous studies showed that the narrowing and deepening of the Yangtze River
103 Estuary resulted in an enhanced longitudinal estuarine circulation (Zhu, 2018), which
104 changed from transversely sheared to vertically sheared. The estuarine stratification
105 was also found to be strengthened, along with an increase in the intensity of lateral
106 circulation. Zhu et al. (2015) investigated the influences of channel deepening and
107 widening on the tidal and nontidal circulations of Tampa Bay, USA, and found that the
108 nontidal circulation was strengthened by these human interventions. However, how
109 does the estuarine circulation respond to both narrowing and deepening/shallowing of
110 the estuary? What happens when the narrowing rate is much larger or smaller than the
111 deepening rate in an estuary? Here the narrowing rate is the ratio of the difference of
112 cross-section widths between two consecutive years divided by the width in the earlier

113 year. Similarly, the deepening rate is the ratio of the difference of water depth in the
114 cross-section between the two consecutive years divided by the earlier year's depth.

115 Here we try to address the above questions by studying the changes in the estuarine
116 circulation from 1977 to 2010 in the Huangmaohai Estuary (HE), a microtidal estuary
117 in the southwest of the Pearl River Delta (PRD), which experienced different stages of
118 topographic changes under human activities: narrowing and deepening (1977-1994, and
119 2003-2010), and narrowing and shallowing (1994-2003). Thus, it provided a good
120 opportunity to study the effect of human activities induced morphological evolution on
121 the estuarine circulation.

122 In this study, we used a state-of-the-art three-dimensional baroclinic model (Delft
123 3d) to simulate the changes in hydrodynamics in the HE in different years and examined
124 the changes in intensities of the longitudinal and lateral estuarine circulations, followed
125 by an analysis of the mechanisms for these changes by conducting diagnostic analyses
126 of the momentum balance. The structure of the rest of the paper is as follows. Section
127 2 introduces the study area and numeral model. Section 3 presents the results of
128 morphological evolution and changes in the estuarine circulation. Then, the
129 mechanisms for the changes in estuarine circulation are investigated using the
130 momentum and vortex balance equations in Section 4. Finally, the conclusions are
131 presented in Section 5.

132

133 **2. Study area and methodology**

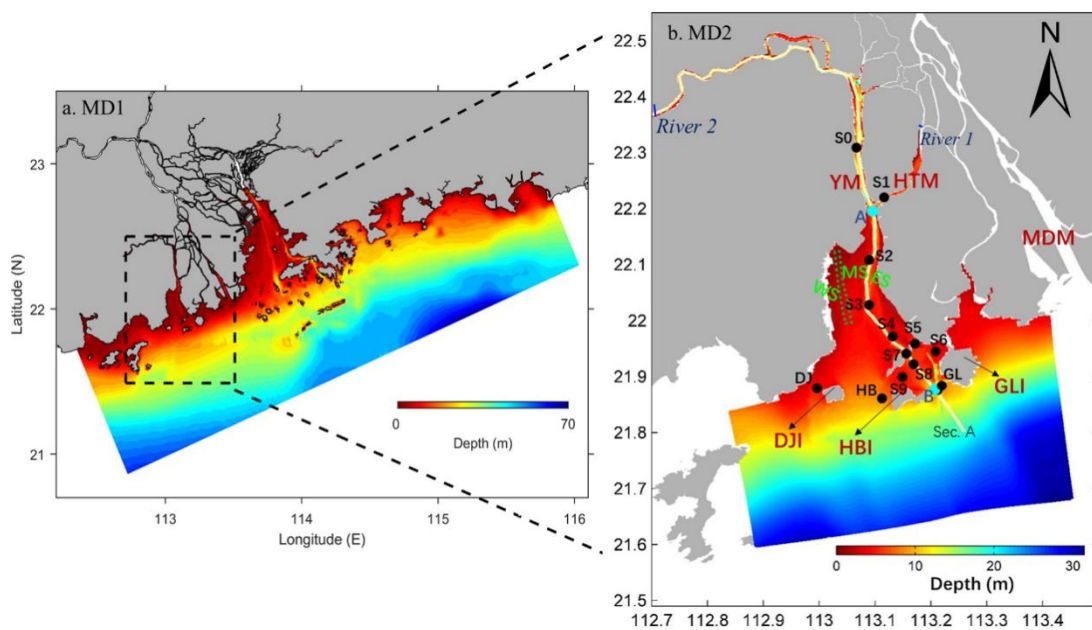
134

135 **2.1 Study area**

136

137 The HE is located in the west of the PRD in southern China and exhibits a
138 distinctly convergent geometry, with a latitude ranging from 21°50' to 22°13' N and
139 a longitude ranging from 113°00' to 113°51' E (Fig. 1). The estuary is composed of a
140 bay (Huangmao Bay) and a tidal river. The bay is trumpet-shaped with an area of 409

141 km². It has a complex bathymetry comprising of two channels and three shoals, namely
 142 the West Channel and East Channel, the West Shoal, Middle Shoal, and East Shoal. In
 143 recent decades, the West Channel is observed to shrink and almost disappear now (Jia
 144 et al., 2012). The width of the bay is 30 km at the estuary mouth and decreases to 1.8
 145 km at the head. The mean water depth of the bay is 4.5 m (Gong et al., 2014). The bay
 146 is connected to the upstream river catchment by two constrictions (Yamen and
 147 Hutiaomen Outlets). Several islands, namely Dajin Island, Hebao Island, and Gaolan
 148 Island, are scattered at the estuary's mouth (shown in Fig. 1b).



149
 150 Fig. 1. The study area (Huangmaohai estuary) and observation stations. Major topographic
 151 features and domains of the nested modeling system over (a) the PRD and (b) the HE and its
 152 adjacent waters. YM = Yamen; HTM = Hutiaomen; MDM = Modaomen; DJI = Dajing Island;
 153 GLI = Gaolan Island; HBI = Hebao Island. The black dots (S0–S9, DJ, HB, and GL) in the
 154 MD2 domain are stations of field deployments in March 2010. The solid lines represent the
 155 along-channel transect (Section A (AB)), which lies in the East Channel. The green dotted lines
 156 represent the West Channel in 1977. Three shoals are shown in (b): West Shoal (WS), Middle
 157 Shoal (MS), and East Shoal (ES).
 158

159 The HE has a subtropical monsoon climate, with the precipitation in the wet season
 160 (from May to September) being high. Approximately 80% of the river discharge occurs
 161 during the wet season, with an average discharge of 200.23 m³/s. The tides in the HE
 162 are mixed semidiurnal with dominant semi-diurnal constituents and smaller diurnal

163 constituents. The tidal range is approximately 1.5 m at the mouth and experiences an
164 initial increase from the mouth towards the head owing to a strong convergence of the
165 bay width. Further landward in the tidal river beyond the bay head, the tidal range
166 decreases by the overwhelming bottom friction (Gong et al., 2012). The tidal current
167 velocity ranges from 0.5 m/s to 1.5 m/s (Huang, 2011), and is higher in deep channels
168 than on shallow shoals. The tidal currents are generally rectilinear in deep channels but
169 become more rotary in shallow shoals.

170 Since the 1980s, human activities have been intense in the HE. A hydroelectric
171 power project upstream of the estuary, channel dredging, sand mining, and construction
172 of Gaolan Island levees have led to great changes in the HE's topography. Also, the HE
173 has rich tidal flat resources and endured frequent reclamation activities. From 1965 to
174 2003, a total of 142.29 km² tidal flat was reclaimed, with an average reclamation rate
175 of 3.74 km²/a, and the reclamation rate continuously but gradually increased during that
176 period. After 2003, the reclamation rate slowed down. In terms of channel dredging,
177 the Yamen Waterway Project was conducted in 1997 to deepen the channel between
178 S0 and S3 in Fig. 1b (Luo, 2010). In April 2005, the Yamen Channel regulation project
179 was implemented to alleviate the serious siltation in the channel, with the channel being
180 dredged to a depth of about 6 m.

181 In the following, we chose 1977, 1994, 2003, and 2010 as the representative years
182 to study the typical scenarios of bathymetric changes in the HE.

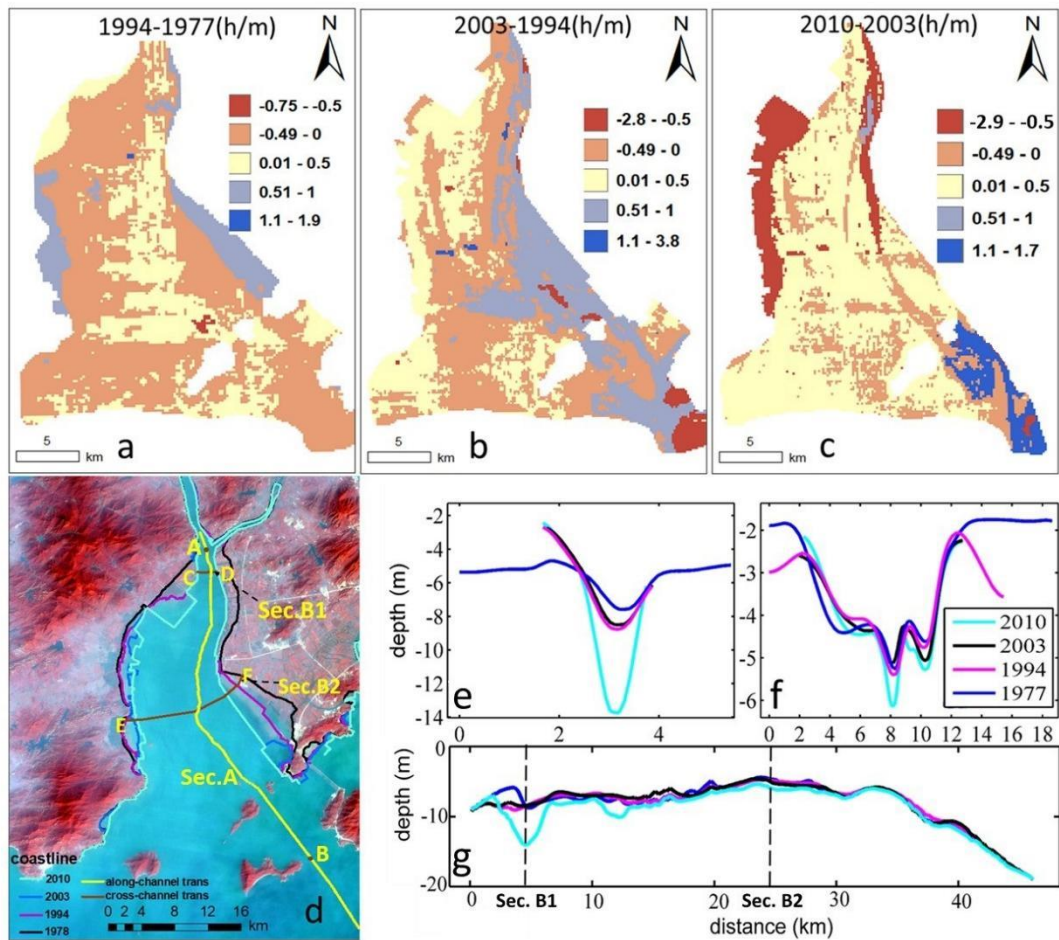
183

184 **2.2 Remote sensing and topographic data**

185

186 Remote sensing data were used for coastline extraction and included Landsat
187 Multi-Spectral Scanner (MSS) data, Landsat Thematic Mapper (TM) data, and Landsat
188 Operational Land Imager (OLI) data. A total of 66 images (Table 1) were downloaded
189 from <http://www.gscloud.cn/>. These data were firstly processed by geometric (with
190 errors less than 0.5 pixels (Ai et al., 2019)) and atmospheric corrections by the ENVI
191 5.3 software. The topography data inside the HE were derived from nautical charts

192 (1977, 1994, 2003, and 2010), published by the Navigation Safety Guarantee Bureau.
 193 The filling and excavation toolbox of ArcGIS was used to calculate the difference
 194 between the volumes in two consecutive periods by superimposing the corresponding
 195 Digital Elevation Models (DEM). We thus obtained the average siltation rates of the
 196 study area over different years (Figs. 2a-c).



197
 198 Fig. 2. (a-c) Water depth difference between two consecutive years ((a)1994-1977; (b)2003-
 199 2003; (c)2010-2003), where the positive value indicates “deepening” and the negative one
 200 indicates “siltation”, (d) Shorelines of 1977-2010 and locations of two cross-sections (AB: Sec.
 201 A; CD: Sec. B1; EF: Sec. B2); (e, f, and g) The bathymetric evolutions at Sections B1, B2, and
 202 A in 1977, 1994, 2003, and 2010.

203
 204 Table 1. Data of remote sensing images

Time	Satellite	Image sensor	Resolution/m	Path/Row	Memory space
1973,1978	Landsat3	MSS	78	122/45	142G
1986-2011	Landsat5	TM	30		

2012	Landsat7	ETM	30
2013-2018	Landsat8	OLR	30

205

206 **2.3 Numerical model setting up and validation**

207

208 The numerical model Delft3d, a fully three-dimensional hydrodynamic water quality
209 model (Lesser et al., 2004), was used to simulate the hydrodynamics in the HE. –Its
210 algorithm can guarantee the conservation of mass, momentum, and energy. The model
211 grid consisted of a nesting grid system, with the MD1 (parent model, Fig. 1a) covering
212 the whole PRD, and the MD2 (child model) covering the HE. For the MD2 model, a
213 curvilinear orthogonal grid of 269*620 was established, with the horizontal resolution
214 ranging from 85 m in the channel to 324 m at the ocean boundary. Vertically, the grid
215 was discretized into 10 layers of σ coordinate. The model system used here is the same
216 as the one in Chen et al. (2020a). The MD1, based on a 1-D (for the river network) and
217 3-D coupled model, covered the whole PRD and the coastal region with a horizontal
218 resolution of 2 km near the open boundary and 500 m inside the PRE (Fig. 1a). The
219 Open sea boundaries for the MD1 comprised hourly tidal elevations and depth-averaged
220 tidal currents derived from nine tidal constituents (M2, S2, N2, K2, K1, O1, P1, Q1,
221 and M4) taken from the global tidal circulation model (TPXO 8,
222 http://volkov.oce.orst.edu/tides/tpxo8_atlas.html) with a resolution of 1/30 ° and daily
223 water elevation, 3-D temperature, salinity (a constant salinity of 34 psu at the open
224 ocean boundary) and velocity data from the Hybrid Coordinate Ocean Model
225 (<https://hycom.org>) with a resolution of 1/12 ° (Chen et al., 2020a). Thus the sources of
226 water level variation and currents at the offshore boundary in MD1 are: 1) tides; 2) non-
227 tidal components by external forcings, such as winds, air pressure, water temperature,
228 and large-scale circulation in the South China Sea. –Briefly, the open boundary
229 conditions of the MD1 model included atmospheric forcing at the water surface, river
230 discharge at the upstream boundary, tidal and non-tidal water elevations and currents,
231 a constant salinity of 34 psu at the open-ocean boundary. The results from the MD1

232 were interpolated to provide ocean boundary conditions for the MD2 model, and there
 233 were no “wind and wave effects” in the MD2.

234 As mentioned above, the hydrodynamics in the HE experiences distinct seasonal
 235 variation. The estuarine circulation during the wet season has been extensively studied
 236 before (Chen et al., 2020a; Chen et al., 2020b). Here we choose the dry season to
 237 investigate the changes in the estuarine circulation caused by topographic changes in
 238 different years. We conducted a series of numerical experiments using the bathymetry
 239 data in 1977, 1994, 2003, and 2010. The simulation time was chosen to be from 00:00
 240 on March 1 to 23:00 on March 31 in the dry season, when observation data were
 241 available in 2010. Field measurements were carried out at 14 mooring stations on
 242 March 17th 17:00 to 18th 22:00, 2010. The measured variables included vertical
 243 profiles of current, temperature, and salinity. In all the four scenarios, two upstream
 244 boundaries were specified (Fig. 1b): at River 2 by specifying real-time water level data
 245 from the MD1 model from 00:00 on March 1, 2010, to 23:00 on March 31, 2010, with
 246 a time interval of 1 hour; At River 1 by specifying a constant river discharge of 100 ms^{-2} .
 247 ². The choice of this constant value was based on previous simulation experiences
 248 (Chen et al., 2020a; Chen et al., 2020b). The salinities at the river inflow boundaries
 249 were set to be 0 psu. The only changing condition of the four scenarios was the
 250 topography (Table 2), so the effect of topographic change can be distinguished. The
 251 measured data from 14 stations in 2010 were used to validate the model.

252
 253 Table 2. Coastline, bathymetries, salinity, flow, and tidal boundary in the four model scenarios.

Scenario	Coastline	Bathymetrie s	The salinity of the open sea	Flow	Tidal boundary
1977/03	1977	1977	2010/03	2010/03	2010/03
1994/03	1994	1994	2010/03	2010/03	2010/03
2003/03	2003	2003	2010/03	2010/03	2010/03
2010/03	2010	2010	2010/03	2010/03	2010/03

255 In this study, the Willmott skill score (SK) was used to evaluate whether the model
 256 result is consistent with the observed data (Willmott, 1981). The SK is defined as:

$$257 \quad SK = 1 - \frac{\sum_{i=1}^n (O_i - M_i)^2}{\sum_{i=1}^n (|M_i - \bar{O}| + |O_i - \bar{O}|)^2}, \quad (1)$$

258 where n is the number of the observed data, M and O are model simulation results
 259 and observations, respectively, and \bar{O} is the average value of the observation data. SK
 260 is used to measure the consistency between the model results and the observations, with
 261 a value between 0 and 1. The larger the value is, the more consistent the simulation
 262 results are with the observed data.

263 Firstly, the water level of the MD2 model was validated. The SKs of the four
 264 observed stations are all above 0.86, indicating that the water level simulation is
 265 reasonable. Secondly, the modeled current directions showed good performance except
 266 for the surface layer at Stations DJ and S0, almost all the SKs are greater than 0.7 (Table
 267 3). The simulation of the current speed is worse than that of the current direction, but
 268 the SKs at most stations are above 0.6, showing a good performance. Lastly, the trends
 269 of observed and simulated salinities are consistent, and almost all the SKs of salinity
 270 validation are above 0.5, especially in S1-S3, showing a good performance of the
 271 salinity simulation.

272 Table 3. Skill scores by comparison of modeled results with observations.

Stations	Current direction			Current speed			Salinity		
	Sur	Mid	Bot	Sur	Mid	Bot	Sur	Mid	Bot
S0	0.18	0.96	0.96	0.77	0.88	0.86	0.32	0.35	0.35
S1	0.94	0.99	0.99	0.65	0.66	0.61	0.94	0.94	0.90
S2	0.78	0.79	0.71	0.83	0.84	0.84	0.84	0.85	0.85
S3	0.87	0.98	0.95	0.34	0.38	0.39	0.92	0.79	0.77
S4	0.84	0.94	0.94	0.53	0.55	0.53	0.77	0.64	0.54
S5	0.86	0.92	0.93	0.66	0.71	0.72	0.37	0.25	0.26
S6	0.79	0.90	0.88	0.68	0.75	0.74	0.15	0.20	0.25
S7	0.82	0.85	0.96	0.74	0.79	0.83	0.86	0.66	0.56
S8	0.84	0.89	0.89	0.59	0.62	0.66	0.82	0.77	0.72
S9	0.80	0.74	0.77	0.54	0.46	0.41	0.59	0.50	0.52
DJ	0.61	0.77	0.77	0.38	0.47	0.51	0.66	0.47	0.37
GL	0.89	0.91	0.93	0.50	0.51	0.49	0.37	0.43	0.41
HB	0.71	0.89	0.89	0.60	0.56	0.56	0.57	0.54	0.53

273

274 As a whole, the simulation of surface currents is worse than that in other layers,
275 since winds and waves were not included in our MD2 model simulations, in which the
276 surface flow is more susceptible to these forcings. The specified river flow at River 2
277 was constant, which may deviate from the real-time data (not available), leading to a
278 poor salinity reproduction at upstream stations. In short, the water level and current are
279 well-validated. The simulation of salinity is generally good, except for some deviations
280 at upstream stations. It shows that the model can reasonably simulate the hydrodynamic
281 processes in the area, and can be used for the following hydrodynamics study in the HE.

282

283 **3. Results**

284

285 **3.1 Morphological evolution**

286

287 Morphological changes between 1977, 1994, 2003, and 2010 are shown in Figs.
288 2a-c. Figure 2a shows that most areas in the HE experienced siltation from 1977 to
289 1994, but the East Channel was deepened by about 0-0.5 m. In the middle of the bay,
290 the nearshore areas were under erosion, and the erosion thickness at the eastern shore
291 was twice that at the western shore. In other areas, the siltation thickness was between
292 0 and 0.5 m. From 1994 to 2003, erosion occurred in the West Shoal, East Channel,
293 East Shoal, and Middle Shoal. Siltation of 0.01-0.5 m happened in the rest of the area,
294 which accounted for most of the HE, so the HE became shallower in 2003. In 2003,
295 siltation in the East Channel was serious and the water depth there became only 2m (Li,
296 2019). From 2003 to 2010, the West Shoal became significantly shallower with a
297 siltation thickness of about 0.5-1m. The East Shoal almost disappeared, and its relict
298 area endured siltation of 1.1-1.7 m, which was mainly due to the construction of coastal
299 protection works. Strong erosion occurred in other areas, especially in the upper bay
300 with a deepening of more than 4m, and the overall water depth of the HE became greater
301 in 2010.

302 Overall, the water depth of the HE changed considerably from 1977 to 2010. It
303 first experienced erosion, then underwent siltation, and followed by erosion again.

304 Figure 2d shows the changes of coastlines for the four representative years. To
305 calculate the rate of geometry convergence, the DSAS tool (Version 5.0) in Arcmap
306 10.3 was used to calculate the end-point rates for cross-shore transects. A more detailed
307 procedure is in Zhang et al. (2019). We chose one longitudinal section along the channel
308 in the estuary and two cross-sections (in Fig. 2d) along the channel for analysis. The
309 longitudinal section (Sec. A) extends from the bay head (point A in Fig. 1b) to the
310 estuary mouth (point B in Fig. 1b), spanning a distance of 50 km. Sec. B1 is located at
311 about 4 km downstream from the bayhead, where the water depth changes sharply in
312 the lateral (or longitudinal) direction (see Fig. 2e). Sec. B2 is approximately 24km
313 downstream from the bayhead and near the null point in the middle of the estuary (see
314 Fig. 2f), and the width of the estuary varied dramatically here (see Fig. 2e). At Sec. A,
315 the water depth near the point of Sec. B1 endured a great change in 2010 due to channel
316 dredging (Fig. 2g). In other periods, the water depth along its course endured gradual
317 deepening. At Sec. B1, the bathymetric change is featured by an increase in water depth
318 and negligible change in width over time. At Sec. B2, both the water depth and width
319 experienced changes from 1977 to 2010, with the depth increased and width decreased
320 (Fig. 2f). The above three sections clearly depict the topographic changes of the estuary
321 in different years.

322

323 **3.2 Changes in the vertically averaged flow and salinity**

324

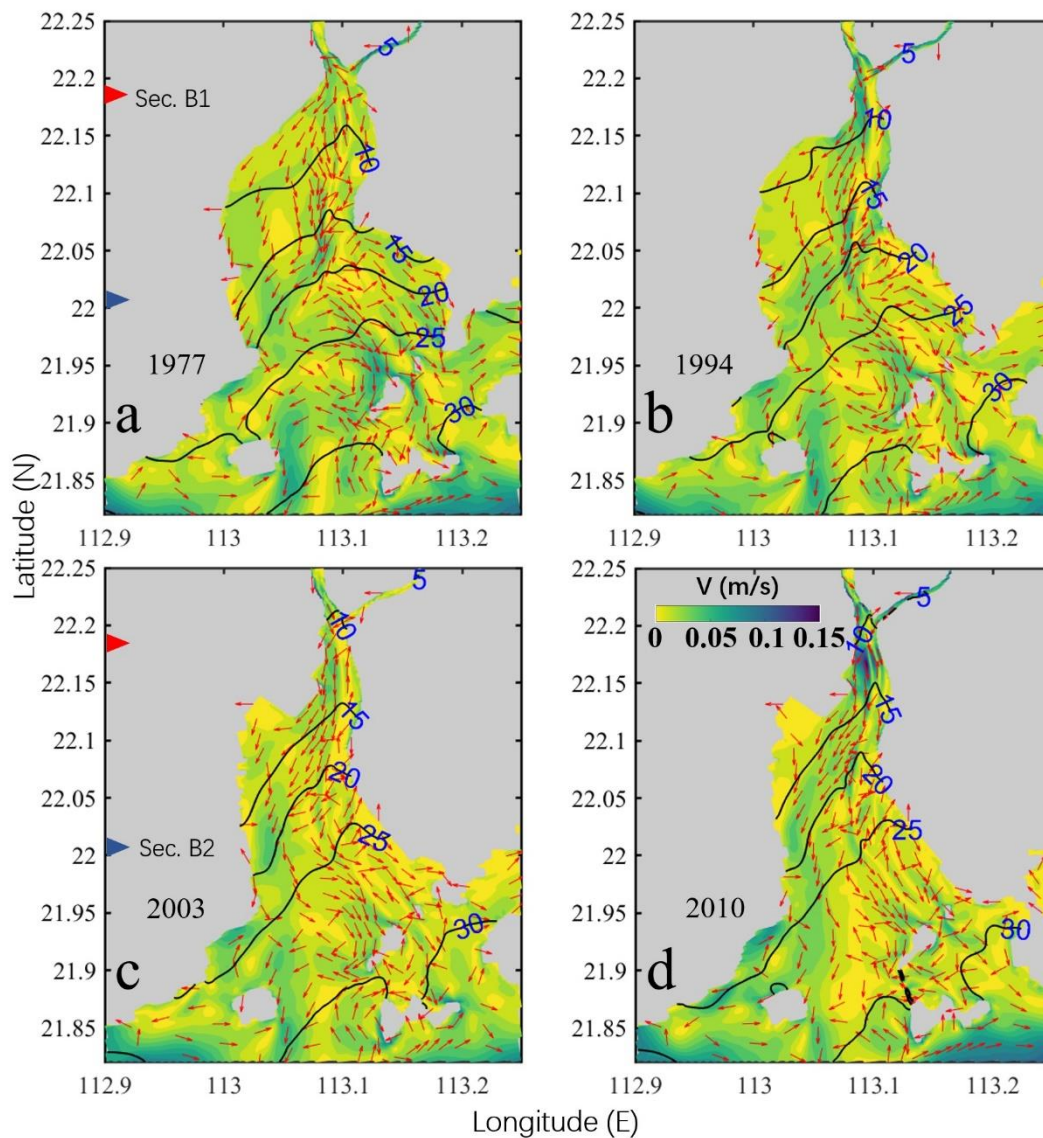
325 Here we present the changes in the tidally and vertically averaged flow and salinity
326 during neap tides in Fig. 3. In 1977 (Fig. 3a), the current speed was generally small,
327 except at the inter-island sections and in the channel. The vertically averaged flow was
328 seaward in the upper bay and the right part of the lower bay (looking landward). It
329 became landward at the left part of the lower bay. In 1994 (Fig. 3b), the current speed
330 was increased in the channel, particularly near Sec.B1. The overall flow pattern was

331 almost similar to that in 1977. In 2003 (Fig. 3c), the flow pattern still kept unchanged
332 when compared to that in previous years. The current speed was decreased relative to
333 that in 1994. In 2010 (Fig. 3d), the seaward flow became more dominant in the upper
334 bay, and more biased southwestward. The seaward flow in the channel was greater than
335 in 2003. The 10 psu isohaline kept moving upstream over time, and reached beyond the
336 bayhead and entered into the tidal river of the estuary in 2010.

337 Overall, we observed that the tidally and vertically averaged flow during neap tides
338 experienced an increase-decrease-increase by the topographic changes, whereas the
339 saltwater consistently intruded more landward.

340 As a supplement, we present the horizontal distributions of tidally averaged
341 surface and bottom circulation and salinity during neap tides for different years in the
342 appendix (Figs. A. 1 and 2). Over the study period, the enhancement of salt intrusion
343 was stronger for the bottom layer and weaker for the surface layer, whereas the increase
344 in residual flow was stronger in the surface layer and weaker in the bottom layer.

345 For the hydrodynamic characteristics of the HE during the flood and ebb tides,
346 Chen et al., (2020a) have investigated the intratidal dynamic processes in detail.



347

348 Fig. 3. Patterns of the ~~tidally and vertically averaged~~~~vertical-averaged-horizantal~~ circulation
 349 during neap tide (from March 10th 00:00 to 11st 00:00 (25h)) in 1977(a1), 1994(a2), 2003(a3),
 350 and 2004(a4). The magnitude of the current is represented by the color shading, while the
 351 current direction is shown by the arrows. The salinity is depicted by the contour lines. The red
 352 and blue triangles depict the positions of two cross-sections (Sec.B1 and Sec.B2).

353

354 3.3 Changes in the estuarine circulation

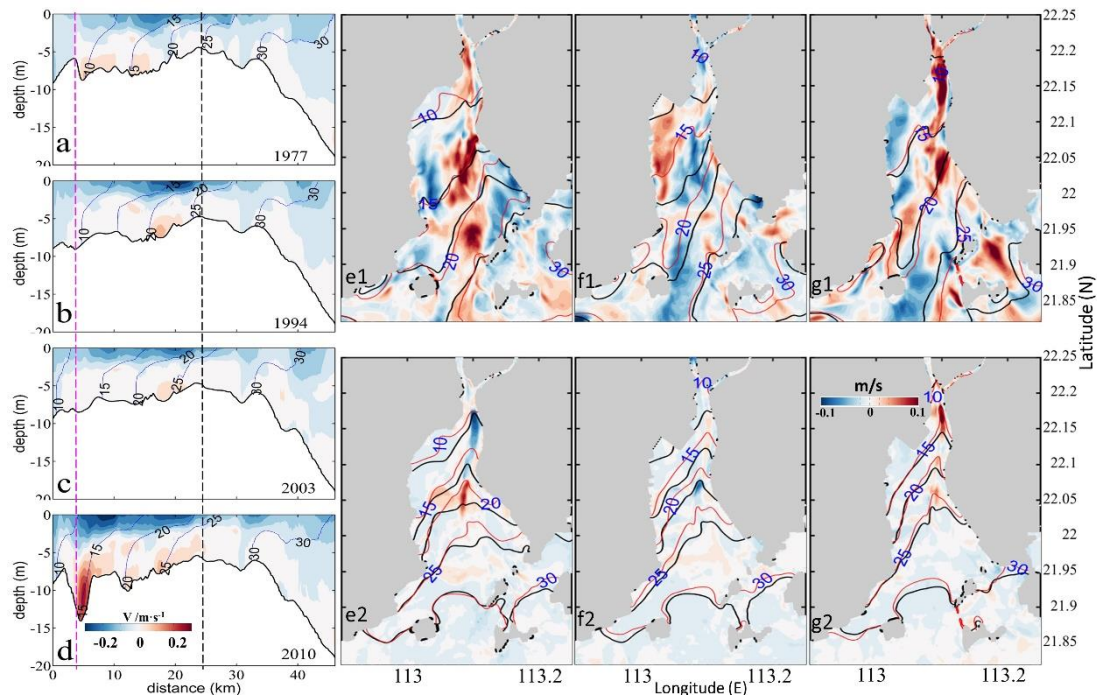
355

356 Figures 4 a-d show that the upper part of the estuary (upstream of the null point)
 357 was highly stratified, and the lower part of the estuary (downstream of the null point)
 358 was well mixed. The classical exchange flow structure was more distinct upstream of

359 the null point. Over time, the surface seaward flow became stronger and more
360 concentrated with the narrowing of the estuary, particularly in 2010. It extended more
361 downstream to near the estuary mouth with the narrowing of the estuary, as evidenced
362 by the extent of the seaward flow of 0.2 m/s. Concomitantly, the bottom landward flow
363 was strengthened and concentrated with the increase in depth. It should be noted that
364 the greatly enhanced estuarine circulation between 3 to 8 km in 2010 (Fig. 4d) could be
365 induced by the intratidal fluctuation of the halocline in response to the large topography
366 change there (Geyer and Nepf, 1996; Chen et al., 2012; Wang et al., 2015) .

367 We also present the changes in the surface and bottom current horizontally. Figs.
368 4e1-g1 show that when the estuary deepened (1977-1994 and 2003-2010), the surface
369 current velocity increased in the channel, and when the estuary shoaled (1994-2003),
370 the surface current velocity in the channel decreased. The changes in the bottom current
371 showed a similar trend (Figs. 4e2-g2), except at the upper part of the channel from 1977
372 to 1994, in which the width was considerably decreased.

373 Along with the change in the longitudinal estuarine circulation, the salt intrusion
374 at Sec. A did not change significantly from 1977 to 1994, but increased from 2003 on,
375 particularly in 2010, when the isohaline of 15 psu reached Sec.B1, whose salinities
376 were less than 12 psu in previous years (Figs. 4a-d). The salt intrusions at the surface
377 and bottom gradually increased with the estuary narrowing (Figs. 4e1-g2).



378

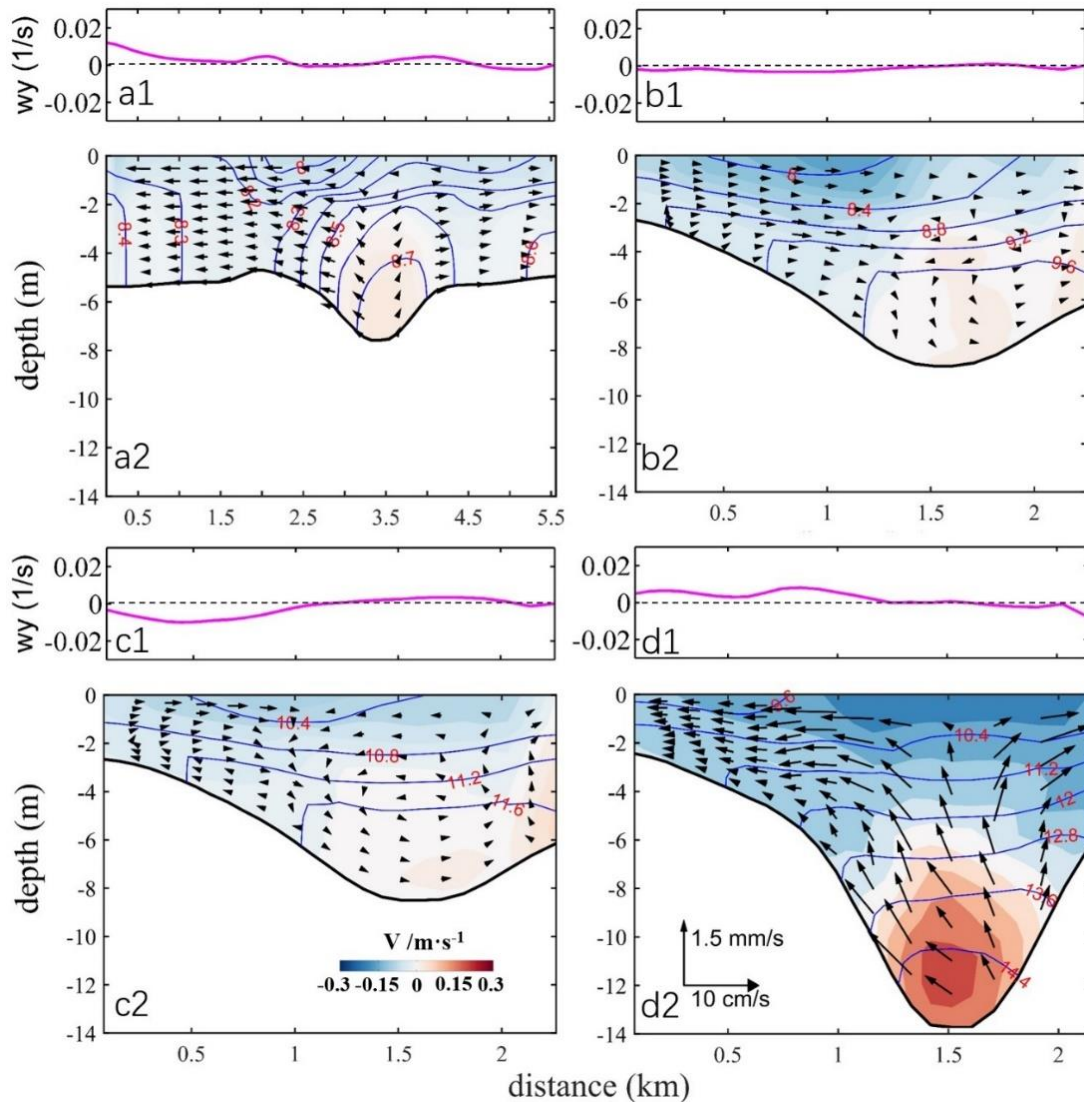
379 Fig. 4. The patterns of the estuarine circulation during the neap tide (from March 10th 00:00 to
 380 11st 00:00 (25h)) in March 1977(a), 1994(b), 2003(c), and 2010(d). The thin lines are the
 381 isolines of salinity in a-d. The pink and black dotted lines represent the locations of Secs. B1
 382 and B2, respectively. The starting point of the X-axis is Point A in Fig. 1b. Surface tidally-
 383 averaged current differences from 1977 to 1994(e1), from 1994 to 2003(f1), and from 2003 to
 384 2010(g1); Bottom tidally-averaged current differences from 1977 to 1994(e2), from 1994 to
 385 2003(f2), and from 2003 to 2010(g2). The red and black lines represent the isolines of salinity
 386 in the later year and the earlier year.

387

388 To analyze the changes of lateral circulation in the estuary, we show the structure
 389 and intensity of the lateral circulation at the two cross-sections (Figs. 5 and 6).

390 At Sec. B1 (Fig. 5), with the increase of water depth, the salinity difference
 391 between the surface and bottom increased, along with an increase in the bottom salinity.
 392 For the lateral circulation, there was no distinct gyre structure in 1977. In 1994, the
 393 lateral flow was dominated by an eastward flow. In 2003, a clockwise vortex was
 394 developed over the West Shoal (0.5-1 km). Meanwhile, an anticlockwise circulation
 395 with smaller vortex intensity was developed in the region of 1-2km from the western
 396 shore. Another clockwise circulation was developed over the East Shoal. When the
 397 estuary became deepened in 2010, the distribution of the lateral circulation was similar

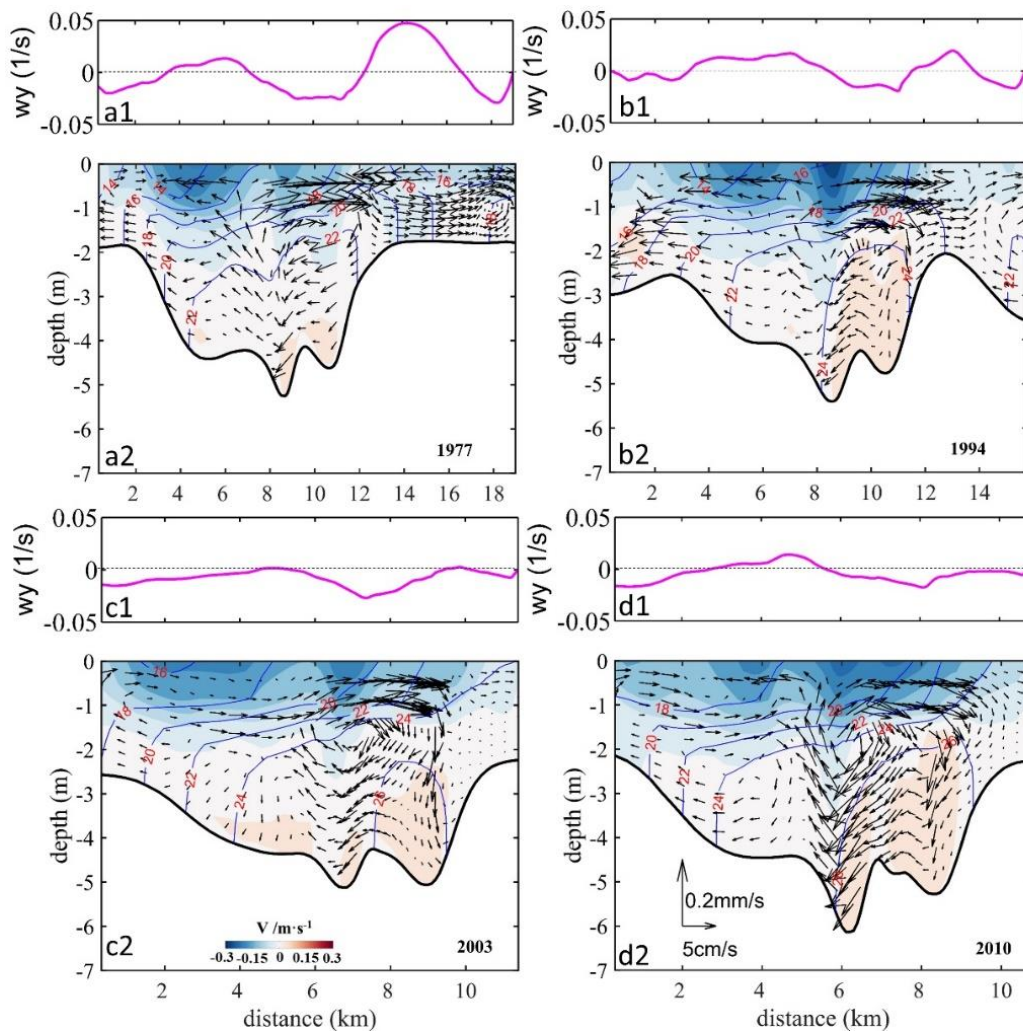
398 to that in 1977, but the vortex intensity increased significantly to about 2-4 times that
 399 of 1977.



400
 401 Fig. 5. The tidally-averaged (from March 10th 00:00 to 11st 00:00 (25h)) lateral circulation and
 402 isohalines (blue lines) at Sec. B1 in 1977(a2), 1994(b2), 2003(c2), and 2010(d2). The starting
 403 point of the X-axis is Point C in Fig. 2d. w_y is the longitudinal vorticity at Sec. B1 in 1977(a1),
 404 1994(a2), 2003(a3), and 2010(a4). The arrows indicate the magnitude of lateral flow and
 405 vertical flow per unit length: 10 cm/s and 1.5 mm/s, respectively.
 406

407 Figure 6 shows the changes in lateral circulation at Sec. B2. With the decrease of
 408 estuary width, the salinity increased in the cross-section over the years. There
 409 developed a clockwise circulation at the right of the deep channel in 1977 and 1994.
 410 This clockwise vortex was seen to move westward from 2003 on. The spatial extent of
 411 the clockwise circulation in the deep channel increased significantly over time.

412 Clockwise vortices developed over the East Shore from 1977 to 2010, but their intensity
 413 became weaker since 2003. In 1977 and 1994, the distance between the deep channel
 414 and the East Shore was greater than 2 km which was sufficient for accommodating
 415 clockwise vortices. From 2003 on, the accommodation space at the East Shore became
 416 limited and restricted the full development of the clockwise vortex. Over the West
 417 Shoal, the lateral circulation pattern showed an anticlockwise circulation in 1977 and
 418 1994. However, since 2003, the lateral circulation over the West Shoal began to develop
 419 a two-cell pattern, with an anticlockwise gyre at the surface and a clockwise one near
 420 the bottom. The clockwise cell developed well in 2010.



421
 422 Fig. 6. The distribution of tidally-averaged (from March 10th 00:00 to 11st 00:00 (25h)) lateral
 423 circulation and isohalines (blue lines) at Sec.B2 in 1977(a2), 1994(b2), 2003(c2), and 2010(d2).
 424 The starting point of the X-axis is Point E in Fig. 2d. w_y is the longitudinal vorticity at Sec.
 425 B2 in 1977(a1), 1994(a2), 2003(a3), and 2010(a4). The arrows indicate the magnitude of lateral
 426 flow and vertical flow per unit length: 5 cm/s and 0.2 mm/s, respectively.

427 As a whole, over the study period, the longitudinal estuarine circulation continued
428 to increase, whereas the lateral circulation experienced varying changes at different
429 cross-sections. At the upstream cross-section (B1), when the estuary narrowed, the
430 original pattern of two-cell vortices with opposite polarity was disrupted. However, it
431 was amplified in 2010 when the water depth was increased. At the cross-section in the
432 middle of the estuary (B2), a similar two-cell pattern was developed. However, in 2003
433 and 2010, the single cell at the West Shoal was split into two cells: an anticlockwise
434 cell at the surface and a clockwise cell at the lower part.

435

436 **3.4 Relationship between the changes in the intensity of estuarine circulation and** 437 **the changes in topography**

438

439 To further quantitatively identify the influence of topographic changes on the
440 estuarine circulation, we calculated the changes in the intensity of estuarine circulations
441 in the longitudinal and lateral directions. The magnitude of estuarine circulation in the
442 longitudinal section was used to represent the intensity of the longitudinal estuarine
443 circulation (Chen and Sanford, 2009). The method was to subtract the subtidal
444 longitudinal velocity of the bottom layer from that on the surface layer. The magnitude
445 of the vorticity in the cross-sections was used to represent the intensity of the lateral
446 circulation (Becherer et al. 2015), and is expressed as:

$$447 \quad w_y = \partial w / \partial x - \partial u / \partial z \quad (2)$$

448 where, w_y is the longitudinal vorticity in the cross-sections. w and u are the
449 currents in the vertical and lateral directions, respectively. $\partial w / \partial x$ is ~~much~~ small and
450 can be ignored, therefore, formula (2) can be simplified as:

$$451 \quad w_y = -\partial u / \partial z \quad (3)$$

452 when w_y is positive, the lateral circulation is an anticlockwise vortex, conversely,

453 when w_y is negative, the lateral circulation is a clockwise vortex.

454 The results of the averaged intensity of estuarine circulation along Sec. A and the
455 averaged intensity of vorticity at the cross-sections are listed in Table 4.

456 Table 4. The changes of width and depth (the maximum depth), area (cross-section area), w-to-
 457 d, narrowing rate, deepening rate, and the intensity of circulations (w-to-d: width-to-depth ratio;
 458 narrowing rate: the ratio of the difference of cross-section widths between two years divided
 459 by the width in the earlier year; deepening rate: the ratio of the difference of water depth in the
 460 cross-section between the corresponding two years divided by the earlier depth. The positive
 461 narrowing rate indicates that the estuary is narrowed; the positive deepening rate indicates that
 462 the estuary is deepened.)
 463

		time	1977/03	1994/03	2003/03	2010/03
Sec.B1	width (km)		5.56	2.25	2.26	2.14
	depth (m)		7.58	8.76	8.50	13.73
	w-to-d		734	257	266	156
	area (km ²)		0.0468	0.0213	0.0207	0.0256
	narrowing rate		\	59.50%	-0.44%	5.30%
	deepening rate		\	15.58%	-2.95%	61.47%
	Sec.B2	width (km)		18.97	15.77	11.40
depth (m)			5.25	5.40	5.12	6.13
w-to-d			3610	2920	2230	1760
area (km ²)			0.0849	0.303	0.0647	0.0646
narrowing rate			\	16.87%	27.71%	5.61%
deepening rate			\	2.86%	-5.19%	19.73%
circulation intensity		longitudinal	Sec. A	0.0274	0.0428	0.0483
	lateral	Sec. B1	0.0111	0.0146	0.0130	0.0278
		Sec. B2	0.0493	0.0460	0.0465	0.0425

464
 465 Table 4 indicates that the longitudinal estuarine circulation intensity increased with
 466 the estuary narrowing, and was largest (0.0594 m/s) in 2010, ~~which was 0.0594 m/s.~~

467 The lateral circulation intensity varied in different cross-sections. For Sec.B1, it
 468 increased gradually when the estuary deepened (from 1994 to 2010). When the
 469 deepening rate reached the maximum (61.47%) in 2010, the lateral circulation intensity
 470 reached the maximum as well. The intensity of lateral circulation increased when the
 471 estuary deepened and narrowed (from 1977 to 1994, and from 2003 to 2010), but it
 472 decreased when the estuary shallowed and narrowed (from 1994 to 2003). For Sec.B2,
 473 the intensity of lateral circulation decreased when the estuary deepened and narrowed
 474 (from 1977 to 1994, and from 2003 to 2010). However, this trend was altered when the
 475 estuary entered into the “narrowing and shallowing period”, with the deepening rate

476 being -5.19%. It indicates that changes in water depth were the dominant factors
 477 affecting the lateral circulation intensity.

478 In general, the relationship between the longitudinal estuarine circulation intensity
 479 and the estuary width showed a monotonic decrease, while that between the
 480 longitudinal estuarine circulation intensity and the water depth is a monotonic increase,
 481 but the lateral circulation intensity seemed to have no simple linear relationship with
 482 the topographic change.

483

484 **4. Discussion**

485

486 **4.1 Contribution of momentum terms to the variation of the longitudinal** 487 **estuarine circulation**

488

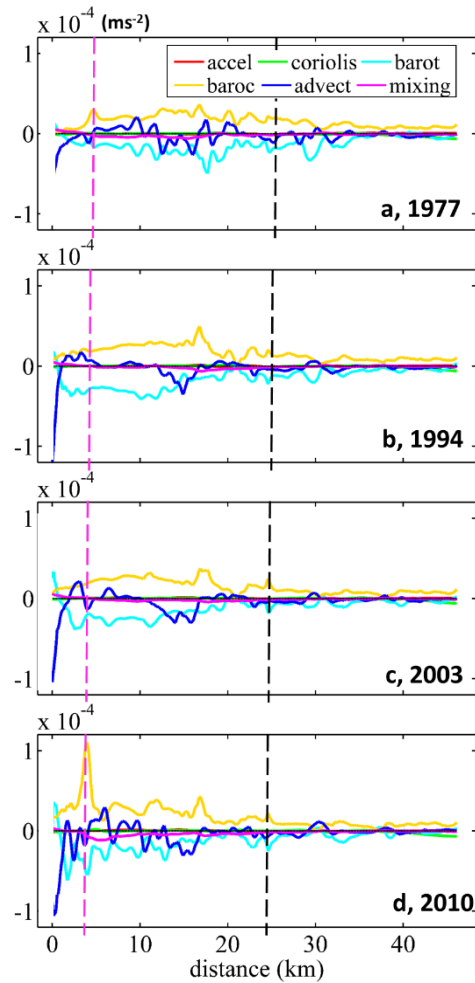
489 To explain the change in the longitudinal estuarine circulation intensity, we
 490 conducted a diagnostic study by examining the changes in terms of the momentum
 491 balance equations. We calculated each term of the momentum equation in the
 492 longitudinal direction in the tidally averaged timescale:

$$493 \quad \frac{\partial v}{\partial t} = \underbrace{f u}_{\text{coriolis}} - \underbrace{g \frac{\partial \eta}{\partial y}}_{\text{barotropic pressure}} - \underbrace{\frac{g z}{\rho_0} \frac{\partial \rho}{\partial y}}_{\text{baroclinic pressure}} - \underbrace{\left(u \frac{\partial v}{\partial x} + v \frac{\partial v}{\partial y} + w \frac{\partial v}{\partial z} \right)}_{\text{advection}} + \underbrace{\frac{\partial}{\partial z} \left(A_v \frac{\partial v}{\partial z} \right)}_{\text{vertical friction}}, \quad (4)$$

494 By comparing the changes in each term and linking them with the characteristics
 495 of morphological evolution, we ~~effort to~~ explain the response of the longitudinal
 496 estuarine circulation to bathymetric change in the perspective of momentum balance.
 497 Though the change in an individual momentum term in Eq. 4 can not represent the
 498 change in the longitudinal estuarine circulation as a whole, it can reflect the change in
 499 the corresponding component for the estuarine circulation (Cheng, 2013). For example,
 500 an increase or decrease in the baroclinic pressure gradient force can reflect the change
 501 in the gravitational circulation, and the change in the advection term is representative
 502 of the change in tidal rectification. In the following, we present the vertically averaged
 503 values for these different terms along the longitudinal section in different years. It
 504 should be noted that the friction term consists of a component of the tidally mean eddy

505 viscosity multiplied by the tidally mean vertical current shear, and a component of the
506 correlation between eddy viscosity and vertical current shear, which is referred to as
507 the tidal straining (Simpson et al., 1990).

508 Figure 7 shows that during the neap tide, the baroclinic pressure gradient force
509 was balanced by barotropic gradient force, friction, and advection term in each year.
510 This is different from the classic estuarine momentum balance (Pritchard, 1956) but
511 consistent with the recent understanding of estuarine physics (Geyer and MacCready,
512 2014). The Coriolis force is quite small as both the latitude of the HE and the residual
513 current are small. The high value of the baroclinic term was observed to shift upstream
514 over time. As the baroclinic term is the multiplication of the salinity gradient and water
515 depth, the changes in this term over years can be induced by the change in water depth
516 and/or the salinity gradient. It can be seen from Fig. 4 that ~~in the~~ north of the null point,
517 the salt intrusion gradually moved towards the bayhead with the estuary narrowing,
518 thus increasing the salinity gradient there. In the meantime, the upstream water depth
519 was increased due to channel dredging, particularly in 2010. Therefore, the increase of
520 the baroclinic ~~force~~ term was caused by both the increases in water depth and salinity
521 gradient. Although the barotropic term contributed a lot to the momentum balance, it
522 did not change obviously with the morphological evolution. The advection term at Sec.
523 B1 increased slightly with the estuary narrowing, especially in the deepening part of
524 the channel in 2010. ~~The friction term was larger in 2010 than in other years~~
525 ~~term at Sec. B1 was the largest in 2010~~, because the salt intrusion increased the vertical
526 shear of the longitudinal current ~~at Sec. B1 there~~. Nevertheless, the increase in friction
527 term was much smaller than that of the baroclinic term. Chant et al. (2018) attributed
528 the increase in exchange flow to the increase in ~~along-channel horizontal~~ salinity
529 gradient and/or a reduction in vertical mixing by deepening, but in our case, the increase
530 in baroclinic term was dominant and the change in vertical mixing even posed a
531 reversed effect.

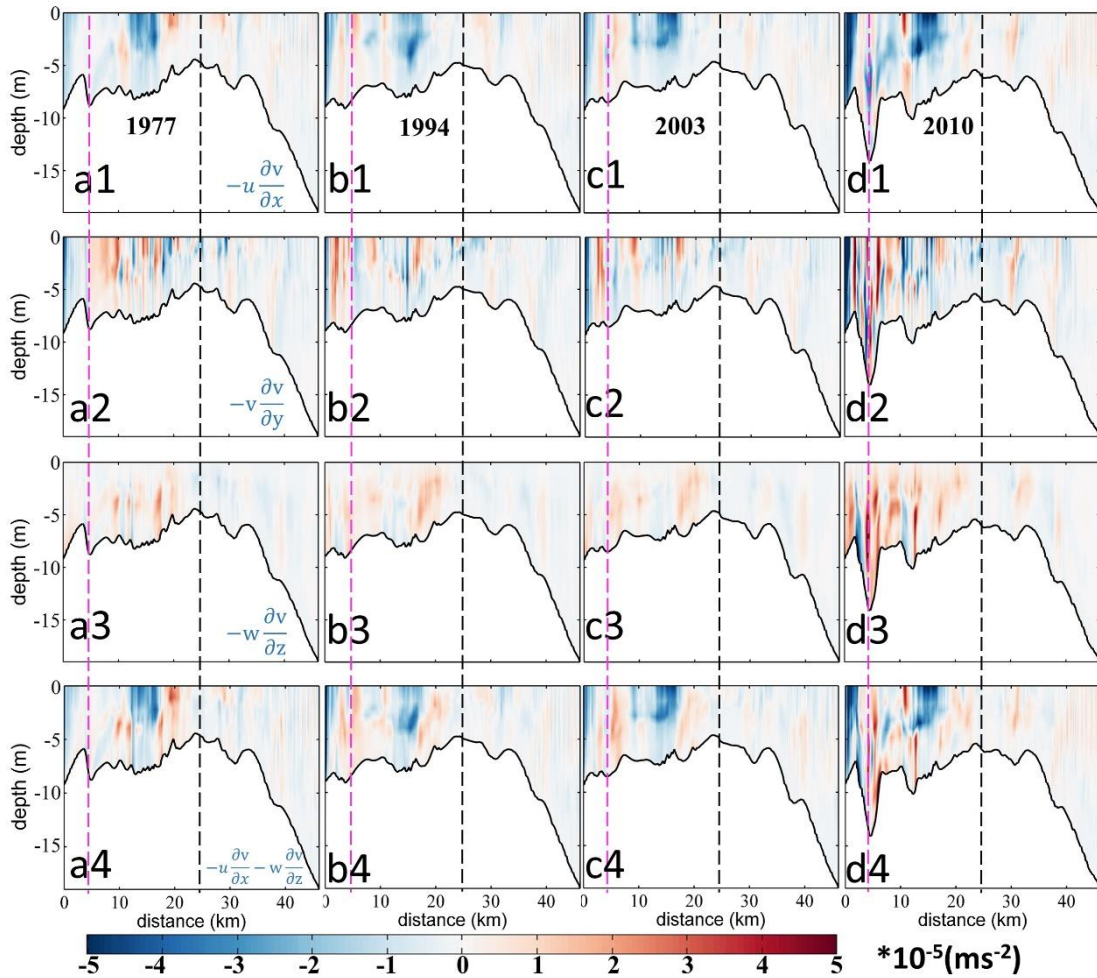


532

533 Fig. 7. Patterns of the tidally-averaged longitudinal momentum terms during neap tide (from
 534 March 10th 00:00 to 11st 00:00 (25h)) at Sec. A in 1977(a), 1994(b), 2003(c), and 2010(d). The
 535 starting point of the X-axis is Point A in Fig. 1b. “accel” in legend: local acceleration term (the
 536 time rate of change of longitudinal flow); “barot” in legend: the barotropic pressure gradient
 537 force ~~term~~; “baroc” in legend: the baroclinic pressure gradient force.

538

539 To further identify the changes in different terms, the advection term was divided
 540 into lateral (X-direction), longitudinal (Y-direction), and vertical (Z-direction)
 541 advection terms (Fig. 8). It is worth noting that the sum of the advection terms in X
 542 and Z directions represents the effect of the lateral circulation.



543

544 Fig. 8. Patterns of the tidally-averaged longitudinal momentum terms during neap tide (from
 545 March 10th 00:00 to 11st 00:00 (25h)) at Sec. A. (a1-d1): The advection in the X direction,
 546 $-u \frac{\partial v}{\partial x}$. (a2-d2): The advection in the Y direction, $-v \frac{\partial v}{\partial y}$. (a3-d3): The advection in the Z
 547 direction, $-w \frac{\partial v}{\partial z}$. (a4-d4): The sum of the advection terms in X and Z directions. 1977, 1994,
 548 2003, and 2010 cases are in the first, second, third, and fourth columns, respectively. The pink
 549 and black dotted lines represent the location of Sec.B1 and Sec.B2, respectively. The starting
 550 point of the X-axis is Point A in Fig. 1b.

551

552 From Fig. 8, in 2010, the advection terms in all directions increased significantly.
 553 Generally, the lateral and vertical advection competes against each other, and their
 554 additive effect is to generate a circulation similar to the gravitational circulation. This
 555 effect was larger the strongest in 2010 than in other years (Figs. 8a4-d4). The
 556 longitudinal advection increased in the upper part of the channel in 2010 (Figs. 8a2-d2),

557 following the deepening and narrowing of the estuary. In the middle of the longitudinal
 558 section, the tidal residual current it induced shows “a seaward flow at the surface and a
 559 landward flow at the bottom”, whereas at in the upper portion, it shows ~~generates~~ a
 560 uniformly landward flow.

561 Overall, from 1977 to 2010, the baroclinic forcing, the friction, and the advection
 562 terms ~~were seen to increase~~ obviously along the Sec. A. The maximum longitudinal
 563 estuarine circulation in 2010 was caused by the increase in the pressure gradient force
 564 and the advection term, especially the baroclinic pressure gradient forcing. ~~We will~~
 565 ~~further discuss~~ The effects of these changes on estuarine circulation will be further
 566 discussed.

567

568 4.2 Analysis of the streamwise vorticity balance for the lateral flow

569

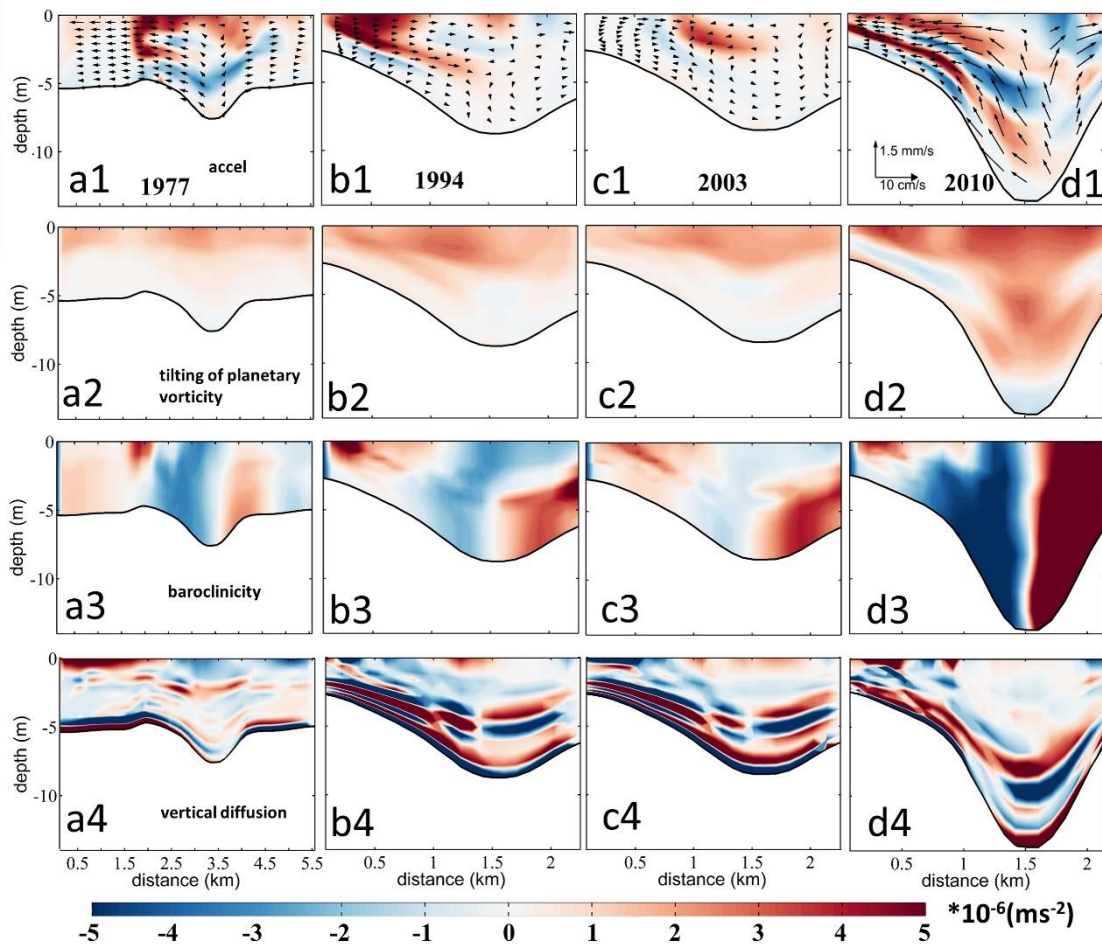
570 In order to reveal the contribution of the vertical shear of the along-channel flow,
 571 the lateral salinity gradient, and the vertical diffusion to changes in the lateral
 572 circulation, we examine the changes in terms of the streamwise vorticity transport
 573 equation (Li et al., 2014):

$$574 \quad \frac{dw_y}{dt} = \underbrace{-f \frac{\partial v}{\partial z}}_{\text{tilting of planetary vorticity}} \underbrace{-g\beta \frac{\partial S}{\partial x}}_{\text{baroclinicity}} + \underbrace{\frac{\partial^2}{\partial z^2}(K_V w_y)}_{\text{vertical diffusion}} + \underbrace{\frac{\partial^2}{\partial x^2}(K_H w_y)}_{\text{horizontal diffusion}}, \quad (5)$$

575 In the right side of Eq. 5, the first term represents the tilting of the planetary
 576 vorticity by vertical shear in the along-channel flow, the second term is the baroclinicity
 577 caused by the lateral salinity gradient, the third term is the vertical diffusion, and the
 578 fourth term is the horizontal diffusion, which is typically two orders of magnitude
 579 smaller than the vertical diffusion term. Therefore, we only show the acceleration and
 580 first three right-hand-side terms in Fig. 9. ~~first four terms in Fig. 9.~~

581 Figure 9 shows that the changes of baroclinicity terms caused by the water depth
 582 change dominated the changes in the lateral circulation at Sec. B1. The baroclinicity
 583 term in the deep channel was generally negative at the left side of the channel, and it
 584 increased significantly in 2010, about 2-3 times the value in 1977. The baroclinicity

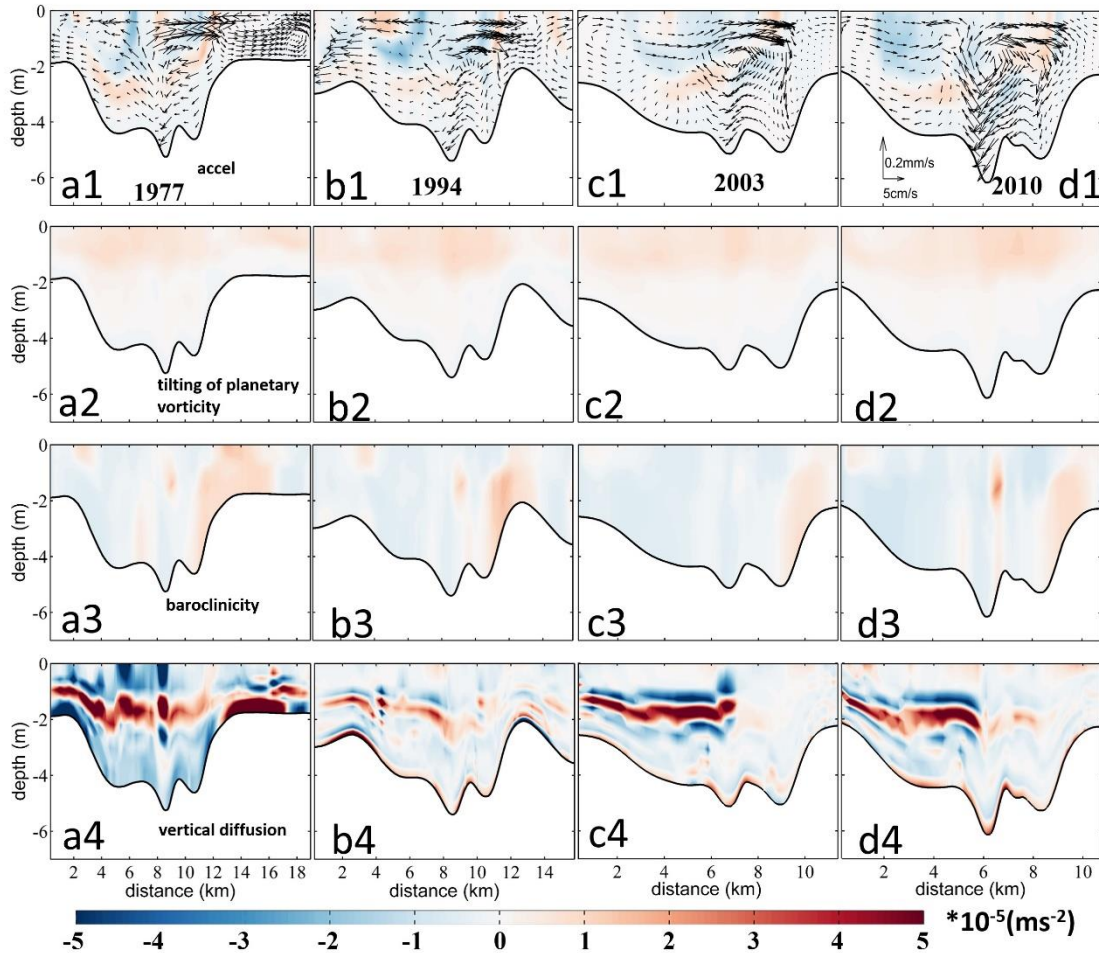
585 term with positive values occurred at the West Shoal over the study period, but the areal
 586 extent occupied by the positive values decreased gradually, with its magnitude
 587 increased obviously in 1994 when the narrowing rate was the largest. A negative
 588 baroclinicity term appeared at the bottom of the West Shoal, indicating that the changes
 589 in water depth can lead to changes in the pattern and magnitude of the baroclinicity
 590 term, which was mainly caused by the changes in the salt intrusion. The tilting of the
 591 planetary vorticity term increased with the estuary narrowing, with the increase in 2010
 592 was greater, which was mostly caused by the depth change. The pattern of the vertical
 593 diffusion term changed significantly in 1977 and 1994, especially at the surface and the
 594 bottom layers of the West Shoal, indicating that it was the changes in width that altered
 595 the vertical diffusion term.



596

597 Fig. 9. Patterns of the tidally-averaged streamwise vorticity equation terms during neap tide
 598 (from March 10th 00:00 to 11st 00:00 (25h)) at Sec. B1. (a1-d1): The local acceleration term
 599 (the time rate of change of the longitudinal vorticity). (a2-d2): The tilting of planetary vorticity

600 term. (a3-d3): The baroclinicity term. (a4-d4): The vertical diffusion term. The cases in 1977,
 601 1994, 2003, and 2010 are in the first, second, third, and fourth columns, respectively. The
 602 starting point of the X-axis is Point C in Fig. 2d. For viewing purposes, the acceleration term is
 603 multiplied by 5. The block arrows in a1-d1 represent the distribution of lateral circulation.
 604



605
 606 Fig. 10. Patterns of the tidally-averaged streamwise vorticity equation terms during neap tide
 607 (from March 10th 00:00 to 11st 00:00 (25h)) at Sec. B2. (a1-d1): The local acceleration term
 608 (the time rate of change of the longitudinal vorticity). (a2-d2): The tilting of planetary vorticity
 609 term. (a3-d3): The baroclinicity term. (a4-d4): The vertical diffusion term. The cases in 1977,
 610 1994, 2003, and 2010 are in the first, second, third, and fourth columns, respectively. The
 611 starting point of the X-axis is Point E in Fig. 2d. For viewing purposes, the acceleration term is
 612 multiplied by 5. The block arrows in a1-d1 represent the distribution of lateral circulation.
 613

614 From Fig. 10, the change in the tilting of the planetary vorticity at Sec. B2 was
 615 analogous to that at Sec. B1. The baroclinicity term did not change much, because the
 616 changes in water depth were smaller in this section. The clockwise circulation over the
 617 West shoal increased as the estuary deepened in 2010, because the baroclinicity term

618 was larger with the increase of salt intrusion and vertical salinity gradient near Sec. B2.
619 The vertical diffusion of the vorticity was overall negative, indicating its effect in
620 dissipating the vorticity. The vertical diffusion term was larger than the baroclinicity
621 term, especially in the middle water, which was inconsistent with the conclusion that
622 the baroclinicity term is the most important one in the lateral circulation (Li et al., 2014).
623 The reason may be that in our study site, the vertical mixing was strong as the estuary
624 became shallow. However, the existence of a pycnocline greatly weakened the
625 momentum exchange between the upper and lower layers: above the pycnocline, the
626 tilting of the planetary vorticity was dominant; whereas, under the pycnocline, the
627 baroclinic term was dominant. The decrease of the estuary width changed the
628 magnitude and pattern of the vertical diffusion term, and the area with a large positive
629 value at the bottom of the East Shoal disappeared, along with the magnitude of the
630 negative value decreased greatly at the easternmost of the section. It indicates that in a
631 shallow estuary, the vertical diffusion term caused by the width change is also important.

632 In Summary, the tilting of the planetary vorticity increased with the decrease of
633 width or with the increase of water depth. The variation of estuary width was
634 responsible for the changes in the vertical diffusion term, and the changes in water depth
635 were responsible for the changes in the baroclinicity term. The increase of the
636 longitudinal estuary circulation can increase the baroclinicity term at the cross-sections
637 by increasing the salinity gradient near the cross-sections, which mainly occurred in the
638 periods of the estuary deepening. The deepening rate of Sec.B1 was the highest (61%)
639 in 2010, which led to the strongest lateral circulation in 2010. The lateral circulation
640 intensity decreased when the estuary narrowed in 2003 due to the decreased
641 baroclinicity term. In addition, the shallowing was the main reason for the pattern
642 change of the lateral circulation at Sec.B2. At Sec. B2, the narrowing rate was the
643 largest in 2003, and the adjustment of the vertical diffusion term resulted in an increased
644 lateral circulation from 1994 to 2003. The decrease of the clockwise circulation at the
645 East Shoal was mainly related to the adjustment of the vertical diffusion term to the
646 baroclinicity term.

647

648 **4.3 Comparison to theoretical results and other estuaries influenced by human** 649 **interventions**

650

651 The longitudinal estuarine circulation is generated by the river discharge, Stokes
652 return flow, longitudinal baroclinic pressure gradient force, tidal straining, and
653 advection (Geyer and Maccready, 2014). The HE features a microtidal tidal regime
654 (tidal range less than 1.5 m), and the component generated by the baroclinic pressure
655 gradient, i.e., the gravitational circulation, would be a primary part of the longitudinal
656 estuarine circulation. The convergent geometry makes it susceptible to the residual flow
657 induced by the longitudinal advection (Burchard et al., 2014). However, as seen above,
658 the horizontal advection (especially the longitudinal advection term) ~~advection~~ also
659 plays a role in generating the estuarine circulation.

660 With channel deepening and width narrowing in the HE, the gravitational
661 circulation was increased by the increased baroclinic pressure gradient force. Based on
662 Geyer's research (2010), the gravitational circulation can be simplified to:

$$663 \quad v_g = a_1(\beta g s_0 R w_0 h_0)^{1/5} U_0^{2/5} w^{-2/5} h^{-1/5}, \quad (6)$$

664 in which w_0 and h_0 is the width and depth at the estuary mouth, respectively. It
665 indicates that the gravitational circulation is inversely related to the water depth and
666 width in the estuary, with a weaker dependence on the water depth. In Chant et al.
667 (2018), the gravitational circulation is completely unrelated to the water depth in their

668 equation (2), which is $v_g \propto \left(\frac{g'R}{w}\right)^{\frac{1}{3}}$, in which the g' is the reduced gravity acceleration.

669 This seems to contradict the situations occurring in many estuaries, such as in the Coos
670 Bay (Eidam et al., 2020), Tampa Bay (Zhu et al., 2015), Changjiang Estuary (Zhu,
671 2018), Ems estuary (Van Maren et al., 2015), Hudson Estuary (Ralston and Geyer,
672 2019), and Newark Bay of the Delaware estuary (Chant et al., 2018). In all these
673 estuaries, the gravitational circulation demonstrated an increase with the deepening of
674 the channel. It suggests that the changes in gravitational circulation vary in different

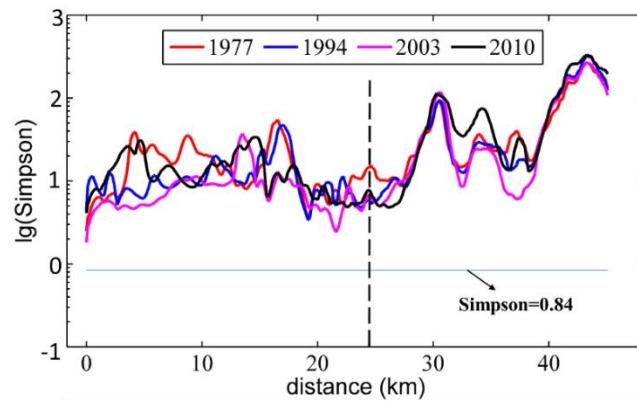
675 parts of the estuary and the longitudinal salinity gradient may not catch up with the
676 change in water depth in the analytical solution, [as](#) proposed by Chant et al. (2018) and
677 Ralston and Geyer (2019). In our study site, the salinity gradient at the upstream part
678 of the longitudinal section was increased owing to an enhanced salt intrusion where
679 water depth increased, which led to an increased gravitational circulation in the
680 ~~upstream of the upper~~ HE (Fig. 4).

681 The tidal straining-induced estuarine circulation is another important component of
682 longitudinal estuarine circulation. The straining-induced circulation is the covariance
683 of the eddy viscosity and the vertical shear of the longitudinal flow (ESCO) in a tidal
684 cycle and is included in the term of internal friction. Cheng et al. (2010) have indicated
685 that ESCO-induced flow dominates the gravitational circulation in periodically
686 stratified estuaries with strong tides, having the same structure as the gravitational
687 circulation. It has the same order of magnitude in weakly stratified estuaries with
688 moderate tides, and is less important in highly stratified estuaries with weak tides, even
689 with a reversed structure with the gravitational circulation. As indicated by Becherer et
690 al. (2015), the strength of the straining-induced circulation is dependent on the Simpson
691 number (or the horizontal Richardson number). The Simpson number is expressed as:

$$692 \quad S_i = g\beta \frac{ds}{dy} \frac{h^2}{u_*}, \quad (7)$$

693 in which u_* is the bottom friction velocity, represented by $u_* = \sqrt{C_d}U_t$, where C_d is
694 the bottom friction coefficient and U_t is the tidal velocity amplitude.

695 When S_i is larger than 0.84, the water column is in a persistent stratified situation,
696 and the straining-induced circulation becomes weaker. We calculated the S_i along the
697 longitudinal section in different years and depict them in Fig. 11.



698

699 Fig. 11. Distribution of the Simpson number in different years along the longitudinal section.
 700 The Y-axis represents the logarithmic of the S_i . The black dotted line represents the location
 701 of the null point.

702 It indicates that along the longitudinal section, the S_i number was mostly above
 703 the criterion of 0.84, showing that the straining-induced circulation is not significant.
 704 The S_i number was the smallest in 2003 and the largest in 2010. It indicates that with
 705 the narrowing and deepening of the HE, the straining-induced circulation became
 706 weaker. This is consistent with Burchard et al. (2014) and Schulz et al. (2015). It
 707 indicates that with the human interventions, the straining-induced circulation became
 708 less important in the longitudinal estuarine circulation.

709 For the advection-induced longitudinal estuarine circulation, we noted that the
 710 longitudinal and vertical advection terms were smaller than the lateral advection. Based
 711 on Cheng and Valle-Levinson (2009), the lateral advection-induced longitudinal
 712 circulation is proportional to the ratio of $h/(wK_m)$, where w is the width, and K_m is
 713 the eddy viscosity. It shows that in a narrower and deeper estuary, the lateral advection
 714 has a larger effect in influencing the longitudinal estuarine circulation. Lerczak and
 715 Geyer (2004) also showed that the effect of the lateral advection on longitudinal
 716 circulation is stronger for narrower estuaries. Our results show that with the narrowing
 717 and deepening of the estuary, not only the lateral advection but also the longitudinal
 718 advection has great influences on the longitudinal estuarine circulation.

719

4.4 The possible future development of the estuarine circulation and its implications

The pattern of lateral circulation during the dry season in the HE experienced a dramatic change from 2003 to 2010 in the West Shoal at Sec. B2, from an under-developed circulation structure to a complete clockwise vortex in 2010. This transition was associated with the increase in lateral salinity gradient, the increase in longitudinal bottom landward flow, and a decrease of friction by the increased water depth and stratification.

The mechanisms for the lateral circulation during the wet season have been revealed by Chen et al. (2020b), who showed that it was primarily driven by the barotropic process, i.e., the water elevation gradient, and thus by the intensity of the ebb jet. Different from the wet season when the river discharge was higher, the lateral circulation in the dry season was more affected by the baroclinic effect. We speculate that, with the narrowing and deepening of the estuary, the lateral circulation ~~even in the wet season~~ will be enhanced even in the wet season accompanied by the ~~strengthened~~ ebb jet in the deep channel strengthened.

In the HE, the channel underwent siltation, and sediment was carried from the channels to side banks by the lateral circulation, making the estuary overall shallower in 2003. In 2005, dredging of the channel increased the channel depth (Luo, 2010), and increased the longitudinal estuarine circulation, though the lateral circulation decreased slightly by the smaller rate of convergence. If reclamation did not occur as frequently as it did in the last century, and the channel dredging continued, the ~~estuarine~~ circulation of ~~the estuary~~HE will ~~in general~~ keep increasing with the increase in the water depth increasing, and thus a positive feedback exists. However, as revealed in Eq. (6) and Eq. (2) in Chant et al. (2018), with the increase in salt intrusion, the longitudinal salinity gradient will decrease, showing negative feedback. Moreover, Schulz et al. (2015) noted that estuarine circulation ~~exhibits~~ a distinct maximum in medium-wide channels by comparing estuarine circulation under different width-to-depth ratios. In

749 our study, as shown in Table 4, the width-to-depth ratio has been decreasing from 1977
750 to 2010, but the estuarine circulation has been increasing. The difference would be
751 caused by the fact that in our study site, the tidal mixing is not strong enough to generate
752 an effective tidal straining-induced circulation.

753 The changes in the estuarine circulation have important implications for sediment
754 transport and morphological evolution in the HE. With the increase of longitudinal
755 estuarine circulation, the sediment trapping effect is expected to be enhanced, thus more
756 riverine sediment would be trapped inside the estuary. In the meantime, the change in
757 lateral circulation would decrease the sediment advection from the channel to the West
758 Shoal, which occurred in the wet season and was favorable for the siltation in the West
759 Shoal (Chen et al., 2020b).

760 Being a micro-tidal partially mixed estuary with standing tidal wave, the estuarine
761 circulation in HE is stronger during the neap tide than during the spring tide. After
762 analyzing the circulation during spring tide, we found the longitudinal circulation
763 reached maximum in 2010 when the water depth was the largest. Similar to the
764 phenomenon during the neap tide, the longitudinal circulation was dominated by the
765 increase in the baroclinicity. However, the changes in the lateral circulation were more
766 complicated than that during the neap tide. In addition to the baroclinicity, the change
767 in vertical diffusion caused by the width change also played an important role. The
768 changes in lateral circulation at the upstream section (Sec. B1) were mostly controlled
769 by the changes in the baroclinicity. On the other hand, the changes in lateral circulation
770 at the downstream section (Sect. B2) were mainly controlled by the changes in the
771 vertical diffusion.

772 In this study, the model used was only driven by river discharge and tides, without
773 considering the effects of winds, waves, sea level rise, and other upstream flows into
774 the estuary. Future work could incorporate the above factors to improve the model's
775 accuracy. Sea level rise can increase the total water depth and inundate more intertidal
776 areas. It has an effect similar to that of channel deepening, to increase the salt intrusion
777 and estuarine circulation. The river flow will be generally decreased in the PRD due to

778 global warming and northward shift of the climate zone. With a decrease of the river
779 discharge, the salt intrusion will be increased and thus the salinity gradient will be
780 decreased, resulting in a weakened estuarine circulation in the HE. For the salinity at
781 the offshore boundary, we are not certain whether it will be increased or decreased. It
782 is influenced by the rain and evaporation, and the large-scale salt transport in the South
783 China Sea. If it increases, the salinity gradient in the HE will be increased, and the
784 estuarine circulation will be enhanced therefore. And vice versa.

785 Definitely, the estuary has undergone natural changes in 40+ years, such as the
786 changes in river inflow, offshore boundary conditions. But as we mentioned, our focus
787 is on the impact of changes in bathymetry on the estuarine circulation, and the paper
788 has already been much lengthy, we leave the effect of other factors for future
789 investigation. It should be noted that our model simulations are not used to reproduce
790 exactly the historical evolution, but to reveal the underlying dynamics.

791

792 **5. Conclusion**

793

794 This study investigated the morphological evolution of the HE from 1977 to 2010
795 using ArcGIS and remote sensing. It was noted that the West Channel of the HE
796 disappeared, causing the morphological pattern to change from “two channels and
797 three shoals” gradually to “one channel and two shoals” throughout the years. Due to
798 the reclamation and development of salt marshes along the estuarine banks, the estuary
799 has been experiencing continuous narrowing. Meanwhile, channel dredging has
800 deepened the estuary over the study period. It had been revealed that the sediment
801 transport pattern changes in response to the changes in river discharge and tidal mixing
802 (Gong et al., 2014). Generally, there exists a sediment convergence zone in the middle
803 of the estuary, and the riverine sediment is trapped inside the estuary to form a
804 turbidity maximum. Our results indicate that the intensity of the longitudinal estuarine
805 circulation kept increasing as the estuary width continued to decrease. The trend of the

806 lateral circulation intensity altered (decreased at Sec. B1 and increased at Sec. B2)
807 when the estuary shallowed (from 1994 to 2003).

808 The changes in the longitudinal estuarine circulation were dominated by the
809 changes in the baroclinic pressure gradient force and advection. As the estuary was
810 narrowing and deepening, the pressure gradient force and advection term (especially
811 the longitudinal advection term) increased, which increased the longitudinal
812 circulation. The change in lateral circulation intensity was mainly caused by the
813 change of the vertical shear of the longitudinal subtidal flow, the lateral salinity
814 gradient, and the vertical dissipation term. The changes in water depth were the
815 dominant factor affecting lateral circulation intensity. The increase of water depth
816 enhanced the longitudinal circulation and the lateral circulation of the upstream cross-
817 section in 2010. The changes in the estuarine circulation have great implications for
818 the sediment transport in the HE, which would be explored in the next step.

819 820 **Data availability**

821 A total of 142G data of 66 images (Table 1) covering the PRD during cloudless days
822 in multiple years (from 1973 to 2018) were downloaded from <http://www.gscloud.cn/>.

823 824 **Author contributions**

825 RuiZhang: Writing - original draft, model runs and analyses. Bo Hong: Writing -
826 review. Lei Zhu: Writing - review. Wenping Gong: Writing - review & editing,
827 Conceptualization, Funding acquisition. Heng Zhang: Visualization, Funding
828 acquisition.

829 830 **Competing interests**

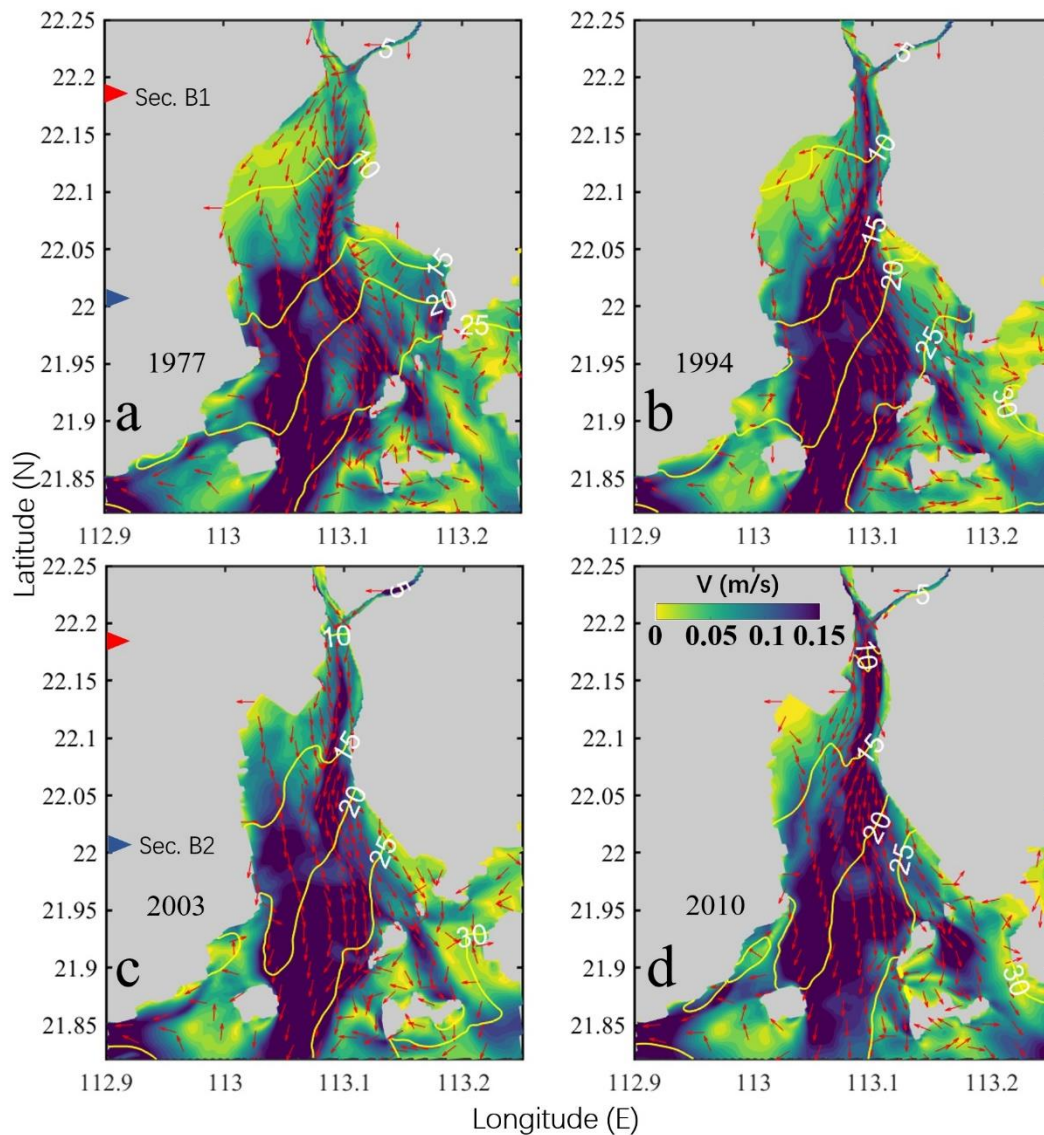
831 The authors declare that they have no conflict of interest.

832 833 **Acknowledgments**

834 This research is funded by the National Natural Science Foundation of China [Grant
 835 nos. 51761135021, 41506102, 41890851]. We would like to thank the National
 836 Aeronautics and Space Administration (NASA) for providing the Landsat remote
 837 sensing data. We are very grateful to graduate students in our team from Sun Yat-sen
 838 for their help in fieldwork and sediment sample analysis in the indoor laboratory.

839

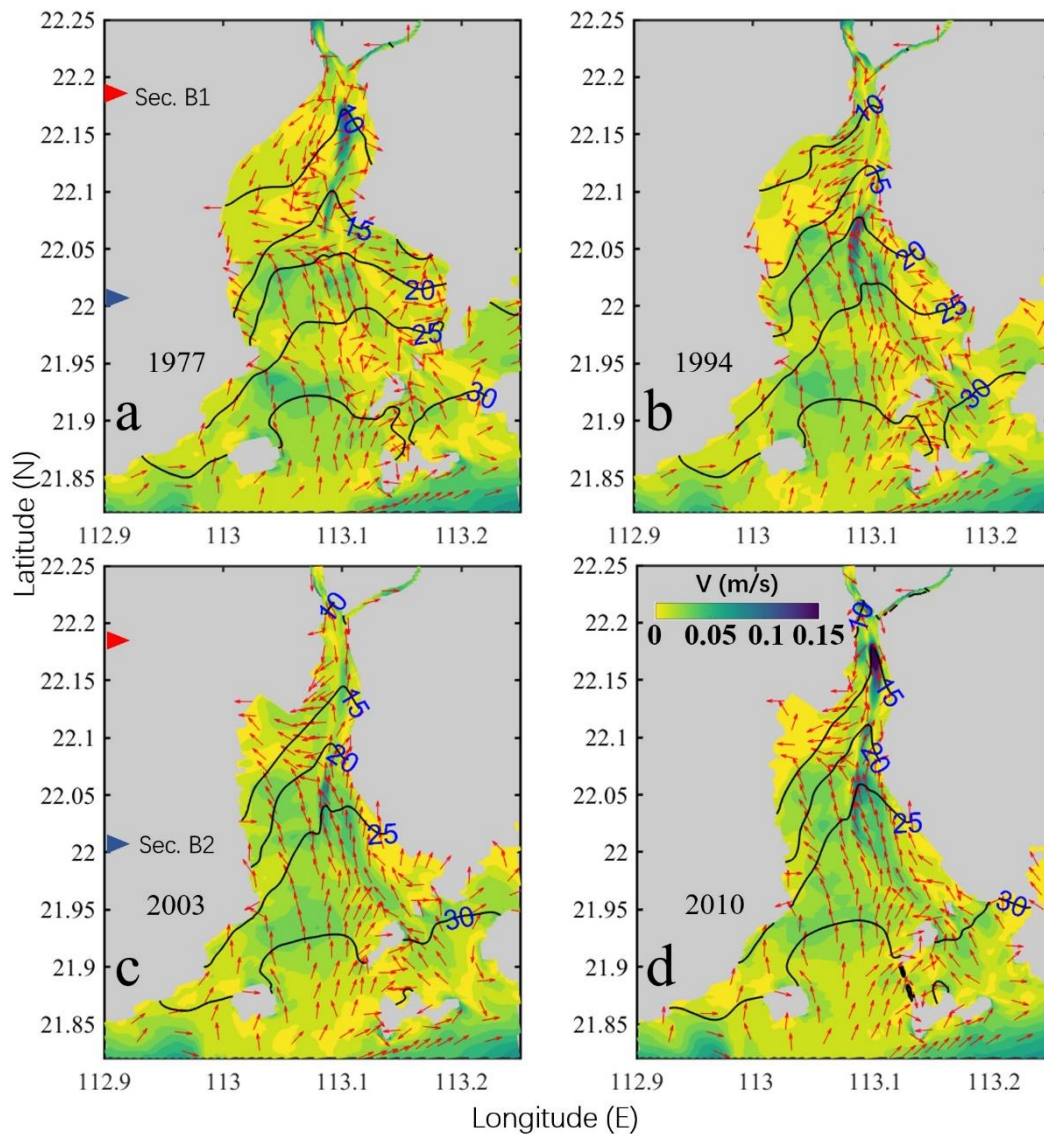
840 **Appendix A**



841

842 Fig. A. 1. Patterns of the tidally and vertically averaged horizontal circulation at the surface
 843 during neap tide (from March 10th 00:00 to 11st 00:00 (25h)) in 1977(a1), 1994(a2), 2003(a3),
 844 and 2004(a4). The magnitude of the current is represented by the color shading, while the

845 current direction is shown by the arrows. The salinity is depicted by the contour lines. The red
 846 and blue triangles depict the positions of two cross-sections (Sec.B1 and Sec.B2).
 847



848
 849 Fig. A. 2. Patterns of the tidally and vertically averaged horizontal circulation at the bottom
 850 during neap tide (from March 10th 00:00 to 11st 00:00 (25h)) in 1977(a1), 1994(a2), 2003(a3),
 851 and 2004(a4). The magnitude of the current is represented by the color shading, while the
 852 current direction is shown by the arrows. The salinity is depicted by the contour lines. The red
 853 and blue triangles denote the positions of two cross-sections (Sec.B1 and Sec.B2).
 854

855 **References**

856
 857 Ai, B., Zhang, R., Zhang, H., Ma, C. L. and Gu, F. G.: Dynamic process and artificial mechanism of
 858 coastline change in the Pearl River Estuary, *Regional Studies in Marine Science*, 30, 100715, 2019.
 859 Amin, M.: On perturbations of harmonic constants in the Thames Estuary, *Geophysical Journal of the*

860 Royal Astronomical Society, 73, 587-603, 1983.

861 Becherer, J., Stacey, M. T., Umlauf, L. and Burchard, H.: Lateral circulation generates flood tide
862 stratification and estuarine exchange flow in a curved tidal inlet, *J. Phys. Oceanogr.*, 45, 638-656,
863 2015.

864 Burchard, H., Hetland, R. D., Schulz, E. and Schuttelaars, H. M.: Drivers of Residual Estuarine
865 Circulation in Tidally Energetic Estuaries: Straight and Irrotational Channels with Parabolic Cross
866 Section, *J. Phys. Oceanogr.*, 41, 548-570, 2010.

867 Burchard, H., Schulz, E. and Schuttelaars, H. M.: Impact of estuarine convergence on residual circulation
868 in tidally energetic estuaries and inlets, *Geophys. Res. Lett.*, 41, 913-919, 2014.

869 Chant, R. J., Sommerfield, C. K. and Talke, S. A.: Impact of channel deepening on tidal and gravitational
870 circulation in a highly engineered estuarine basin, *Estuar. Coast.*, 41, 1587-1600, 2018.

871 Chen, L. H., Gong, W. P., Scully, M. E., Zhang, H., Cheng, W. C. and Li, W.: Axial wind effects on
872 stratification and longitudinal sediment transport in a convergent estuary during wet season, *Journal*
873 *of Geophysical Research: Oceans*, 125, e2019J-e15254J, 2020a.

874 Chen, L. H., Gong, W. P., Zhang, H., Zhu, L. and Cheng, W. C.: Lateral circulation and associated
875 sediment transport in a convergent estuary, *Journal of Geophysical Research: Oceans*, 125, e2019J-
876 e15926J, 2020b.

877 Chen, S. N., Geyer, W. R., Ralston, D. K. and Lerczak, J. A.: Estuarine Exchange Flow Quantified with
878 Isohaline Coordinates: Contrasting Long and Short Estuaries, *J.phys.oceanogr*, 42, 748-763, 2012.

879 Chen, S. N. and Sanford, L. P.: Axial Wind Effects on Stratification and Longitudinal Salt Transport in
880 an Idealized, Partially Mixed Estuary, *J. Phys. Oceanogr.*, 39, 1905-1920, 10.1175/2009JPO4016.1,
881 2009.

882 Cheng, P.: Decomposition of Residual Circulation in Estuaries, *Journal of Atmospheric & Oceanic*
883 *Technology*, 31, 698-713, 2013.

884 Cheng, P. and Valle-Levinson, A.: Influence of lateral advection on residual currents in microtidal
885 estuaries, *J. Phys. Oceanogr.*, 39, 3177-3190, 2009.

886 Cheng, P., Valle-Levinson, A. and De Swart, H. E.: Residual currents induced by asymmetric tidal
887 mixing in weakly stratified narrow estuaries, *J. Phys. Oceanogr.*, 40, 2135-2147, 2010.

888 Chernetsky, A. S., Schuttelaars, H. M. and Talke, S. A.: The Effect of Tidal Asymmetry and Temporal
889 Settling Lag on Sediment Trapping in Tidal Estuaries, *Ocean Dynam.*, 60, 1219-1241, 2010.

890 Dyer, K. R. 1977. Lateral circulation effects in estuaries. *National Academy of Sciences*, p. 22-29.

891 Eidam, E. F., Sutherland, D. A., Ralston, D. K., Dye, B., Conroy, T., Schmitt, J., Ruggiero, P. and Wood,
892 J.: Impacts of 150 Years of Shoreline and Bathymetric Change in the Coos Estuary, Oregon, USA,
893 *Estuar. Coast.*, 1-19, 2020.

894 Fischer, H. B.: Mixing and Dispersion in Estuaries, *Annu. Rev. Fluid Mech.*, 8, 107-133,
895 10.1146/annurev.fl.08.010176.000543, 1976.

896 Geyer, W. R.: Estuarine salinity structure and circulation, *Contemporary issues in estuarine physics*, 12,
897 26, 2010.

898 Geyer, W. R. and Maccready, P.: The Estuarine Circulation, *Annu. Rev. Fluid Mech.*, 46, 175-197, 2014.

899 Geyer, W. R. and Nepf, H.: Tidal pumping of salt in a moderately stratified estuary, *Coastal and estuarine*
900 *studies*, 213-226, 1996.

901 Gong, W. P., Jia, L. W., Shen, J. and Liu, J. T.: Sediment transport in response to changes in river
902 discharge and tidal mixing in a funnel-shaped micro-tidal estuary, *Cont. Shelf Res.*, 76, 89-107,

903 2014.

904 Gong, W. P., Liu, H., Ren, J. and Yu, H. B.: The study of tidal propagation in the Huangmaohai estuary
905 and its underlying mechanisms, *Acta Oceanol. Sin.*, 34, 41-54, 2012.

906 Gong, W. P., Schuttelaars, H. and Zhang, H.: Tidal asymmetry in a funnel-shaped estuary with mixed
907 semidiurnal tides, *Ocean Dynam.*, 66, 637-658, 2016.

908 Huang, T. 2011. Study on abnormal changes of tidal range in the huangmaohai estuary. Guangdong
909 Water Resources and Hydropower, Guangzhou, China.

910 Jia, L. W., Luo, J. and Ren, J.: The analysis of the evolution of a sand bar and its formation in the
911 Huangmao Bay in the Pearl River Delta, *Acta Oceanol. Sin.*, 34, 120-127, 2012.

912 Kjerfve, B., Stevenson, L. H., Proehl, J. A., Chrzanowski, T. H. and Kitchens, W. M.: Estimation of
913 material fluxes in an estuarine cross section: A critical analysis of spatial measurement density and
914 errors 1, *Limnol. Oceanogr.*, 26, 325-335, 1981.

915 Lacy, J. R., Stacey, M. T., Burau, J. R. and Monismith, S. G.: Interaction of lateral baroclinic forcing and
916 turbulence in an estuary, *Journal of Geophysical Research: Oceans*, 108, 1-34,
917 <https://doi.org/10.1029/2002JC001392>, 2003.

918 Lerczak, J. A. and Rockwell Geyer, W.: Modeling the Lateral Circulation in Straight, Stratified
919 Estuaries*, *J. Phys. Oceanogr.*, 34, 1410-1428, 2004.

920 Lesser, G. R., Roelvink, J. V., Van Kester, J. and Stelling, G. S.: Development and validation of a three-
921 dimensional morphological model, *Coast. Eng.*, 51, 883-915, 2004.

922 Li, C. Y. and O'Donnell, J.: Tidally driven residual circulation in shallow estuaries with lateral depth
923 variation, *Journal of Geophysical Research Oceans*, 102, 27915-27929, 1997.

924 Li, M., Cheng, P., Chant, R. J., Valle-Levinson, A. and Arnott, K.: Analysis of vortex dynamics of lateral
925 circulation in a straight tidal estuary, *J. Phys. Oceanogr.*, 44, 2779-2795, 2014.

926 Li, W., Shi, J. Z., Pu, X. and Hu, G. D.: Circulation within curved channel of the north passage in the
927 changjiang river estuary: a vorticity approach, *Oceanologia et Limnologia Sinica*, 48, 682-694, 2017.

928 Li, Y. B. 2019. Numerical simulation of the formation and evolution of the geomorphic characteristics
929 of Huangmao Sea. Dalian University of Technology, Dalian, China.

930 Luo, J. 2010. Cause Analysis of Morphological evolution of Huangmao sea Estuary in the Decade to
931 Century-scale. Sun Yat-sen university, Guangzhou, China.

932 Pritchard, D. W.: Salinity distribution and circulation in the Chesapeake Bay estuarine system.. 1, *Mar.*
933 *Res*, 11, 106-123, 1952.

934 Pritchard, D. W.: The dynamic structure of a coastal plain estuary, *J Marine Res*, 15, 33-42, 1956.

935 Ralston, D. K. and Geyer, W. R.: Response to channel deepening of the salinity intrusion, estuarine
936 circulation, and stratification in an urbanized estuary, *Journal of Geophysical Research: Oceans*,
937 124, 4784-4802, 2019.

938 Salles, P., Valle-Levinson, A., Sottolichio, A. and Senechal, N.: Wind - driven modifications to the
939 residual circulation in an ebb - tidal delta: Arcachon Lagoon, Southwestern France, *Journal of*
940 *Geophysical Research Oceans*, 120, 728-740, 2015.

941 Schulz, E., Schuttelaars, H. M., Gr We, U. and Burchard, H.: Impact of the depth-to-width ratio of
942 periodically stratified tidal channels on the estuarine circulation, *J. Phys. Oceanogr.*, 45, 411804097,
943 2015.

944 Scully, M. E., Geyer, W. R. and Lerczak, J. A.: The Influence of Lateral Advection on the Residual
945 Estuarine Circulation: A Numerical Modeling Study of the Hudson River Estuary, *J. Phys.*

946 Oceanogr., 39, 107-124, 10.1175/2008JPO3952.1, 2009.

947 Scully, M. E., Geyer, W. R. and Lerczak, J. A.: The Influence of Lateral Advection on the Residual
948 Estuarine Circulation: A Numerical Modeling Study of the Hudson River Estuary, *J. Phys.*
949 *Oceanogr.*, 39, 107-124, 10.1175/2008JPO3952.1, 2009.

950 Scully, M., Friedrichs, C. and Brubaker, J.: Control of estuarine stratification and mixing by wind-
951 induced straining of the estuarine density field, *Estuaries*, 28, 321-326, 10.1007/BF02693915, 2005.

952 Simpson, J. H., Brown, J., Matthews, J. and Allen, G.: Tidal straining, density currents, and stirring in
953 the control of estuarine stratification, *Estuaries*, 13, 125-132, 10.2307/1351581, 1990.

954 Van Maren, D. S., van Kessel, T., Cronin, K. and Sittoni, L.: The impact of channel deepening and
955 dredging on estuarine sediment concentration, *Cont. Shelf Res.*, 95, 1-14, 2015.

956 Wang, T., Geyer, W. R., Engel, P., Jiang, W. S. and Feng, S. Z.: Mechanisms of Tidal Oscillatory Salt
957 Transport in a Partially Stratified Estuary, *J. Phys. Oceanogr.*, 45, 2773-2789, 2015.

958 Waterhouse, A., Tutak, B., Valle-Levinson, A. and Sheng, Y.: Influence of Two Tropical Storms on the
959 Residual Flow in a Subtropical Tidal Inlet, *Estuar. Coast.*, 36, 1037-1053, 10.1007/s12237-013-
960 9606-3, 2013.

961 Willmott, C. J.: On the validation of models, *Phys. Geogr.*, 2, 184-194, 1981.

962 Wilson, R. and Filadelfo, R. 1986. Subtidal Current Variability in the Lower Hudson Estuary. Springer -
963 Verlag, Berlin, Germany. p. 132-142.

964 Winterwerp, J. C.: Fine sediment transport by tidal asymmetry in the high-concentrated Ems River:
965 indications for a regime shift in response to channel deepening, *Ocean Dynam.*, 61, 203-215, 2011.

966 Zhang, R., Chen, L. H., Liu, S. S., Zhang, H. and Lin, G. Y.: Shoreline evolution in an embayed beach
967 adjacent to tidal inlet: The impact of anthropogenic activities, *Geomorphology*, 346, 106856, 2019.

968 Zhu, J., Weisberg, R. H., Zheng, L. Y. and Han, S. Z.: Influences of Channel Deepening and Widening
969 on the Tidal and Nontidal Circulations of Tampa Bay, *Estuaries & Coasts*, 38, 132-150, 2015.

970 Zhu, L. 2018. Alteration of estuarine circulation under the inference of morphological evolution. East
971 China Normal University, Shanghai, China.

972